### Title

Physical and chemical template-blocking strategies in the exponential amplification reaction of circulating microRNAs




### Journal

Analytical and Bioanalytical Chemistry, 412(11)

### ISSN

1618-2642



### Authors

Trinh, Michael P
Carballo, Jocelyn G
Adkins, Gary B
et al.



### Publication Date

2020-04-01

### DOI

10.1007/s00216-020-02496-w

Peer reviewed

Published in final edited form as:

*Anal Bioanal Chem*. 2020 April ; 412(11): 2399–2412. doi:10.1007/s00216-020-02496-w.

# Physical and Chemical Template-Blocking Strategies in the Exponential Amplification Reaction of Circulating MicroRNAs

**Michael P. Trinh**[1], **Jocelyn G. Carballo**[1], **Gary B. Adkins**[1], **Kaizhu Guo**[1], **Wenwan Zhong**[1,*]

[1]Department of Chemistry, University of California-Riverside, Riverside, CA 92521, USA

## Abstract

The detection of circulating miRNA through isothermal amplification wields many attractive advantages over traditional methods, such as reverse transcription RT-qPCR. However, it is challenging to control the background signal produced in the absence of target, which severely hampers applications of such methods for detecting low abundance targets in complex biological samples. In the present work, we employed both the cobalt oxyhydroxide (CoOOH) nanoflakes and the chemical modification of hexanediol to block non-specific template elongation in exponential amplification reaction (EXPAR). Adsorption by the CoOOH nanoflakes and the hexanediol modification at the 3' end effectively prevented no-target polymerization on the template itself and thus greatly improved the performance of EXPAR, detecting as low as 10 aM of several miRNA targets, including *miR*-16, *miR*-21, and *miR*-122, with the fluorescent DNA staining dye of SYBR Gold™. Little to no cross-reactivity was observed from the interfering strands present in 10-fold excess. Besides contributing to background reduction, the CoOOH nanoflakes strongly adsorbed nucleic acids and isolated them from a complex sample matrix, thus permitting successful detection of the target miRNA in serum. We expect the simple but sensitive template-blocking EXPAR could be a valuable tool to help discovery and validation of miRNA markers in biospecimens.

## Graphical Abstract



*Corresponding author: wenwan.zhong@ucr.edu.



The study used human serum purchased from a commercial source, which has been determined by the Office of Research Integrity and the Institutional Review Board of University of California Riverside as research activity not involved human subject. Experiments were performed in accordance with the ethical standards.

**Conflicts of interest** The authors have no competing interests to declare.

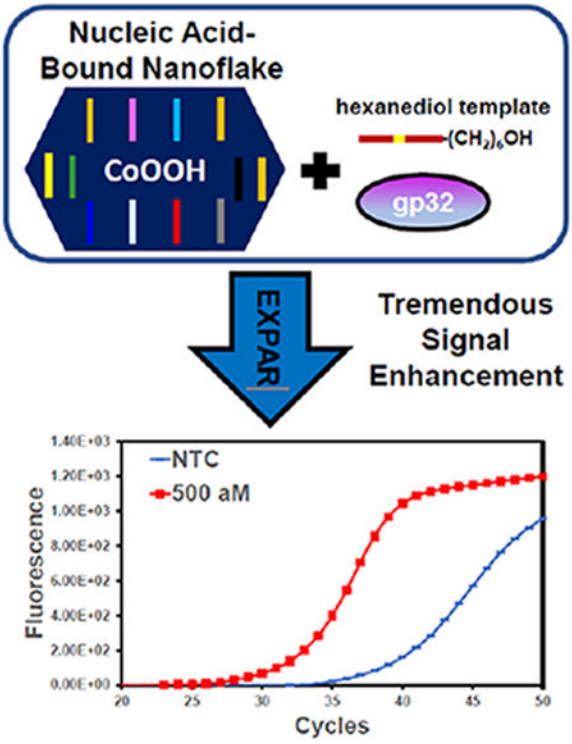


**Keywords**

exponential amplification reaction; EXPAR; isothermal amplification; CoOOH nanoflakes; microRNA; detection; serum; cancer

## Introduction

Cancer is one of the greatest health challenges faced by mankind worldwide, but it is manageable and susceptible during its early developmental stages. Therefore, advancements in early cancer detection have contributed greatly to improving survival rates in the past decades. One promising strategy is to detect biomarkers in biofluids, such as blood, urine, saliva, etc. Liquid biopsy is less invasive, much easier and cheaper to procure than sampling tumor tissues[1]. Among the deluge of identifiable biomarkers present in biofluids, circulating microRNAs (miRNAs) have inspired the close examination of cancer research, owing to their 1) regulatory involvement in a variety of biological processes[2], 2) altered expression during cancer[3–7], and 3) resistance to degradation in body fluids due to the protection bestowed by RNA-binding proteins and vesicles[8–10].

Bringing detection of miRNAs in biofluids into feasibility needs to overcome the forefront challenge presented by their very low abundance in biofluids. Additionally, the physiological matrix contains large amounts of interfering molecules[11,12] that can readily generate false positives. Detection of circulating miRNA also needs to be practical and accurate under low-resource contexts, where rapid assay times, small sample consumption, portability and affordability are immensely valued. These requirements cannot be easily met by

conventional methods like real-time quantitative polymerase chain reaction (RT-qPCR), Northern blot, microarray, and next-generation sequencing, all of which are considered gold standards and still widely employed in research labs, but have poor sensitivity, consume expensive reagents, and offer low throughput[13–16]. Thus, on-going technology developments have been striving to amend these issues for general clinical applications and simplify the assay demands for field conditions, with isothermal amplification catching great attention and showing high promise.

Isothermal amplification utilizes the target nucleic acid to trigger reaction cascades that amplify the detection signals[17]. The reaction can involve no enzymes, such as in hybridization chain reaction (HCR); or rely on enzymes, like in loop-mediated isothermal amplification (LAMP), strand displacement amplification (SDA), helicase-dependent amplification (HDA), rolling circle amplification (RCA), and nicking enzyme amplification reaction (NEAR). The enzyme-assisted reactions are more rapid and sensitive compared to the enzyme-free approaches, but generally require more optimization and are vulnerable to enzyme instability. Nevertheless, high background generation is a perpetuating dilemma in isothermal amplification and is the main culprit of poor signal-to-noise for both amplification approaches[18–20]. The root cause of background is from the undesirable template-polymerase [21] or self-priming template interactions[22].

Nanomaterials with unique chemical or optical properties can be added to enhance signal amplification, and possibly also serve as analyte enrichment platforms by taking advantage of their unique features in fluorescence quenching and specific affinity to single-stranded nucleic acids. The most widely employed nanomaterials are gold nanoparticles (AuNPs)[23–25], metal oxides [26,27] and graphene oxide (GO)[28–30], with the transition metal dichalcogenide (TMD)[31–35] monolayers recently emerging. TMDs have outperformed AuNPs and GO in sensor design because they incorporate large atoms in their 2D infrastructure, which can help shuttle electron transportation and enhance the performance of electrochemical or optical sensors[36]. Metal oxides, like CoO, reported by Liu *et al.* [26,27] also exhibit strong quenching and DNA adsorption capacities, but DNA desorption for downstream processing could be challenging. On the other hand, cobalt oxyhydroxide (CoOOH) nanoflakes [37–39] are a two-dimensional nanomaterial with versatile functions, including the ability to bind strongly to single-stranded (ss) nucleic acids but only partially to double-stranded (ds) ones, as well as catalyze the oxidation of peroxidase substrates in the presence of H2O2.

Exponential amplification reaction (EXPAR) uses the strand displacement activity of a thermostable polymerase and a nickase to achieve multiple rounds of strand extension for high amplification efficiency. Compared to the aforementioned enzyme-assisted isothermal techniques, EXPAR is arguably simpler by using only a linear two-unit X'–X' template, whereas others tend to deploy hairpin-like probes that invite secondary structures; and it also has a high enzyme turnover rate[40]. However, the high amplification efficiency of EXPAR also renders high false-positive amplification. In the present work, this problem was solved by using a combination of chemical and physical template-blocking approaches: modification at the 3' end with hexanediol, and adsorption of the template by the ssDNA-binding CoOOH nanoflakes. Together with the ssDNA-binding protein of T4 gp32, these

elements synergistically increased the positive signal and decreased the nonspecific polymerase activity, resulting in greatly improved detection sensitivity and specificity, compared to other chemical labels and other ssDNA-binding nanomaterials. Ultimately through the developed method, successful detection of several miRNAs was attained. In addition, the nanoflakes can adsorb the single-stranded nucleic acids and thus enrich the analyte of interest from biofluids, thereby avoiding the interference from matrix components in the amplification reaction. Detection of miRNAs in serum was then realized without pre-purification.

## Experimental section

### Oligonucleotides and reagents.

All oligonucleotides were synthesized, purified, and purchased from Integrated DNA Technologies (Coralville, IA). The sequences used are enumerated in Table S1 and their designs were assisted with tools in NUPACK (www.nupack.org) and DINAMelt (http://unafold.rna.albany.edu/). All enzymes, proteins, and the NEBuffer 3.1 were procured from New England Biolabs (Ipswich, MA). Glycerol and dNTP mix were purchased from Promega Corporation (Madison, WI). SYBR™ Gold Nucleic Acid Gel Stain (10,000x concentrate in DMSO) was obtained from Thermo Fisher Scientific Inc. (Waltham, MA). CoOOH nanoflakes were synthesized and purified in-house. Single-donor serum was purchased from Innovative Research Inc. Gold nanospheres were purchased from nanoComposix (San Diego, CA). Graphene oxide sheets were obtained from the Nanotechnology Health Implications Research Consortium established by the National Institute of Environmental Health Sciences (NIEHS)[41,42]. All dilutions were prepared using ultrapure water unless otherwise stated.

### CoOOH nanoflake fabrication.

To 1,650 μL of ultrapure $H_2O$, 150 μL of 100 mM $COCl_2$ hexahydrate and 75 μL of 5 M NaOH were added sequentially and sonicated together for 10 minutes. After the elapsed time, 75 μL of 0.9 M NaCIO were added and the resulting brown solution was allowed to continue incubating under sonication for 30 more minutes. The CoOOH nanoflakes were then pelleted by centrifugation at 10,000 RCF for 10 minutes. Upon removing the supernatant, the nano flake pelleted was rinsed twice vigorously with 1.5 mL of ultrapure water by vortexing and sonicating, and a third time with 1.5 mL of ethanol. The nanoflakes were recovered during these wash steps by centrifugation at 10,000 RCF for 10 minutes. The purified nanoflakes were then desiccated by briefly baking them in 60 – 80 °C and subsequently leaving them under house vacuum until visibly dry. Finally, the nanoflakes were weighed and dispersed in ultrapure water to the desired concentration.

### CoOOH nanoflake characterization.

The morphology of the CoOOH nanoflakes was determined on an FEI Tecnai T12 transmission electron microscope at 120 kV after mounting them onto a Formvar/carbon film on a 400 mesh copper grid and the average vertex-to-vertex length of each nanoflake was measured by Fiji. Atomic force microscopy (AFM) was carried out on 0.21 mm thick AFM mica discs using Veeco Dimension 5000 and nanoflake thickness was inferred from

NanoScope® Analysis software (Bruker). The zeta potential was obtained from a Delsa™ Nano C Particle Analyzer (Beckman Coulter). Fourier transform infrared (FTIR) absorption spectrum was measured on a Nicolet 6700 FT-IR spectrometer (Thermo Fisher Scientific) using nanoflakes prepared as a 1% w/w KBr pellet that was oven-dried at 110 °C for at least 24 hours. For UV-vis characterization, a 1 μg/μL solution of nanoflakes was prepared and the corresponding spectrum was collected in a Varian Cary® 50 UV-Vis spectrometer (Agilent Technologies Inc.).

To assess RNA adsorption, 100 ng of ssRNA ladder was incubated with 0, 1, 3 or 5 μg of nano flakes over ice for at least 10 minutes. The supernatant was recovered by centrifugation at 10,000 RCF and analyzed by 5% PAGE. To determine the loading capacity of the nanoflakes, Fiji was utilized to quantify and convert the band intensities to an adsorption percentage. Target RNA adsorption by the nanoflakes was evaluated by fluorescence quenching, which was performed by mixing together 10 pmol each of target RNA and FAM-labeled capture probe, along with 100 μg of CoOOH nanoflakes, in a total volume of 100 μL constituted by 1× TE buffer (10 mM Tris, 0.1 mM EDTA, pH 8.0). Fluorescence measurements were carried out in the PTI QuantaMaster™ 400 (HORIBA) fluorometer.

### Template-blocking EXPAR for detection of miRNAs.

Template-blocking EXPAR was performed in a one-pot reaction manner. One μL of miRNA target was added to the detection mix that contained 0.8 μL of 1 μM EXPAR template (hexanediol), 0.8 μL of 10 mM dNTP mix, 1 μL of 1 μg/μL CoOOH nanoflakes, 2 μL of 10× NEBuffer 3.1, 2 μL of 10× SYBR™ Gold, 2 μL of 100% glycerol, and 6.4 μL of ultrapure $H_2O$. Then, the enzyme mix containing 1 μL of 1.6 U/μL *Bst* 2.0 DNA polymerase, 1 μL of 10 U/μL *Nt.BstNBI* nicking enzyme, and 2 μL of 20 μM T4 gp32 was added and aspirated gently to homogenize the solution.

The EXPAR reaction was monitored in low profile, non-skirted, 96-well PCR plates (Thermo Scientific) and controlled using a Bio-Rad (Hercules, CA) CFX Connect Real-Time PCR Detection System. Isothermal amplification was initiated at 55 °C and each cycle was defined as 30 seconds. The fluorescence data was exported using the Bio-Rad CFX Manager software. By matching their cycle numbers, the fluorescence values of each target or nonspecific strand were normalized to the corresponding background fluorescence in order to obtain the signal-to-noise (S/N) ratios. The highest S/N was then identified for the true target of the reaction and fluorescence values were assigned to each strand and control using the cycle corresponding to the highest S/N.

### EXPAR application in serum.

Off-the-clot single donor human serum (Innovative Research Inc.) was first clarified by briefly centrifuging at 10,000 RCF and transferring the supernatant to a clean tube while heeding large debris particles. Spiked serum samples were then prepared by diluting 5 μL of miRNA with 5 μL of clarified serum. Three μg of CoOOH nano flakes were added to the serum and incubated for at least 10 minutes over ice with occasional agitation. The nanoflakes were then pelleted by centrifugation at 10,000 RCF for at least 5 minutes, separated from the serum supernatant and rinsed once with 1× PBS. After pelleting the

nanoflakes once again at 10,000 RCF, the wash solution was discarded and the pellets were allowed to rest on ice. The nucleic acid-bound nanoflakes were then mixed with the detection solution, which was prepared in the same way as in the template-blocking EXPAR, but supplied with 2 μL ultrapure $H_2O$ instead of nanoflakes to get the final reaction volume of 20 μL. The resulting solution was sonicated until the nanoflakes were completely dissolved. Upon subsequent addition of the enzyme mix, the full reaction was monitored on a Bio-Rad CFX Connect Real-Time PCR Detection System.

### Polyacrylamide gel electrophoresis.

Denaturing urea polyacrylamide gel electrophoresis (PAGE) was used to analyze the nucleic acid species present in EXPAR. For analyzing species of 20 – 100 bases, 20% acrylamide was the final gel composition while 5% was prepared for 50 – 1000 bases. PAGE was run with 1× TBE buffer at 100 V initially for band focusing and 150 V or more for the remaining time. The gel was stained in lx SYBR Gold and imaged on a Spectroline™ Slimline™ UV Transilluminator (Fisher Scientific).

## Results and discussion

### Design of template-blocking EXPAR.

Individual circulating miRNA from healthy human serum can be as low as tens of fM[43], although the total miRNA concentration can reach a few pM[44]. To detect such a low content of the miRNA target, the simple but highly sensitive isothermal EXPAR approach is attractive. However, high background signal resulting from the no-target self-extension of the EXPAR template could be a big challenge, particularly if the DNA staining dyes are employed as the cost-effective detection method. The presence of a large amount of endogenous proteins[12] in serum can also interfere with enzymatic amplification.

We propose that CoOOH nanoflakes can help reduce the background in EXPAR because they have high affinity to single-stranded nucleic acids, as demonstrated in our work and others' [37,38]. The CoOOH nanoflakes have large specific surface areas and rich positive surface charges, attracting the negatively charged nucleic acids. Their preference for single-stranded nucleic acids to double-stranded duplexes stems from the stronger interaction between the unpaired nucleobases and the nanoflake surface via π–π stacking and H-bonding. Thus, they can bind to the single-stranded EXPAR template to increase the space hindrance for template-polymerase interactions, thereby pacifying template self-extension and reducing background. In addition, they can adsorb and isolate the microRNAs from the complex sample matrix, so that detection by EXPAR can be carried out in a clean solution without interference from the matrix components. The physical template blockage with the nanoflakes can collaborate with chemical modification and protein binding on the template to further improve the signal-to-noise ratio.

The scheme of template-blocking EXPAR is illustrated in Figure 1. Firstly, the single-stranded nucleic acids in the sample are adsorbed by the nanoflakes. Secondly, the nanoflakes are transferred to the EXPAR reaction matrix containing the chemically modified template. Next, the templates are hybridized to the target miRNA strands to unload them off

the nanoflake for insolution enzymatic reaction, while the free ones are adsorbed on the nanoflake surface, preventing their interaction with the polymerase to generate non-target amplification. The insolution amplification is the same as the conventional EXPAR design: the polymerase extends the target miRNA and the nicking enzyme generates a break on the double-stranded product for another cycle of isothermal strand extension and displacement, producing multiple copies of ssDNA detected by the fluorescence stain of SYBR Gold™.

### Target and enzyme selection.

The present work developed the template-blocking EXPAR to mainly target *miR-122* and miR-16 and miR-21 were also targeted to demonstrate the wide applicability of our method. *miR-122* is a well-established biomarker for liver toxicity[45–49], and is also downregulated in liver diseases, such as Hepatitis B & C[49,50] and hepatocellular carcinoma[45,46]. It is also a potential marker upregulated in patients with breast cancer[51,52], because it regulates glucose metabolism that is important for tumor cell adaptation to microenvironments. Frequent downregulation[53] and upregulation[54] of *miR*-16 and -21 have been reported to be closely related to cancer development in a wide variety of tissues and organs, including breast, lung, brain, and many others[43,53,55–58]. With the highly significant clinical relevance and disease implications entailed in these miRNAs, an isothermal assay that can rapidly quantify their abundance in biological matrices with simple procedures will be highly beneficial for validating their roles as diagnostic markers in different diseases. However, while many isothermal methods have been reported for detection of *miR*-16 and -21 [59–63], relatively few assays have been developed so far for circulating *miR*-122[64–66].

The *Bst* homologues, *Bst* 2.0, *Bst* 2.0 WarmStart, and *Bst* 3.0, are *in silico* designs based on *Bst* Large Fragment but with improved processivity and thermostability. They are good polymerase choices for EXPAR because of their high strand-displacement activity and capability to extend from RNA primers and nicks. In addition, their optimal operation temperature range of 55 – 65 °C can help diminish template secondary structures and minimize target-template mismatches to improve assay specificity. These enzymes were tested initially for amplification of 500 aM miR-122, with *Bst* 2.0 outperforming the other *Bst* enzymes and resulting in the highest S/N value (see Electronic Supplementary Material (ESM) Fig. S1). With *Bst* 2.0 being the optimal polymerase used in our design, *Nt.BstNBI* was selected for nick generation because it can operate at 55 °C to match the optimal temperature of *Bst* 2.0.

### CoOOH nanoflake characterization and nucleic acid binding capability.

The nanoflakes were fabricated by oxidizing C0CI2 under basic conditions. They were rigorously characterized to verify their correct fabrication. The signature –O–H and –O–Co–O– IR stretches at 3421.3 $cm^{-1}$ and 584.9 $cm^{-1}$, respectively, were observed in the FTIR spectrum (ESM Fig. S2a). These stretching frequencies reflect the hydroxyl-functionalized surface of the nanoflakes and the $Co–O^{2-}$ complex in the oxide, proving successful preparation of the nanoflake. The nanoflakes were also imaged by TEM and showed a single-layer hexagonal morphology with an estimated vertex-to-vertex length of 158.98 ± 36.75 nm (Figure 2a). The average thickness of the nanoflake was assessed by AFM and

found to be about 1.47 ± 0.20 nm (Figure 2a). The zeta-potential of the nanoflakes was measured as 33.39 ± 1.02 mV. Both the rigid 2D planar geometry and positive surface charges support that the nanoflakes provide a large relative surface area ideal for nucleic acid adsorption through electrostatic attraction.

The ability to differentiate between single- and double-stranded nucleic acids is a defining trait of CoOOH nanoflakes to assist EXPAR in our design. The absorption spectrum of the nanoflakes exhibited a broad peak in the visible light range of 450 – 550 nm (ESM Fig. S2b), indicating their capability to quench green fluorescent dyes, like fluorescein, if the dye is within the energy transfer distance to the nanoflake surface. Utilizing this feature, we incubated a FAM-labeled capture probe with the nanoflakes and evaluated fluorescence quenching by the nanoflakes to estimate their affinity to the DNA probe. We found that 96% of the probe fluorescence was quenched by the nanoflakes, and the addition of an equimolar complementary target miRNA recovered about 24% of the fluorescence (Figure 2b; ESM Fig. S3a), confirming that the nanoflakes prefer the single-stranded nucleic acids over the double-stranded ones.

Besides binding to the EXPAR template for background reduction, we also expect the nanoflakes to be able to extract microRNAs from sample matrices. Thus, the capability of the CoOOH nanoflakes for binding of ssRNAs was tested by incubating increasing nanoflake amounts with 100 ng of the ssRNA ladder. Afterward, the nanoflakes were pelleted and the supernatant was analyzed by PAGE. We found that with 1 pg nanoflakes, the band intensity for RNAs shorter than or equal to 150 nt started to decrease until they disappeared completely with the addition of 5 pg nanoflakes (ESM Fig. S3b). Using the band intensities, we calculated the bound ratio and determined that 1 pg nanoflakes could adsorb up to 13.16 ng of RNA, which is sufficiently greater than the total RNA in 50 μL of healthy human serum[44]. The adsorption behavior also has an apparent bias toward shorter RNA strands: the intensity of the higher MW bands also decreased but to lesser extents than the lower MW ones—a suitable property for the isolation and detection of miRNA (ESM Fig. S3b).

### Template blockage for background reduction.

In order to bring out the best performance of CoOOH nanoflakes, we first determined the proper amounts of nanoflakes and templates for the reaction because the nanoflakes may also bind to the ssDNA products displaced off the template during polymerization, rendering them undetectable by SYBR Gold™. Thus, sufficient nanoflakes should be provided to adsorb the templates, but not in excess to quench the product signal. We evaluated the EXPAR performance for *miR*-122 using a 53-nt template that contained two complementary sequences flanked by a 9-nt Nt.BstNBI recognition site (ESM Table S1). We found that the optimal amount of CoOOH nanoflakes for our reaction was 1 μg since this amount yielded the largest separation between background and target amplification curves (ESM Fig. S3c). As a result, we employed this amount in the following tests.

To gain a better understanding of our background issue, we briefly compared the performance of EXPAR using an unmodified or modified template alone, or using an unmodified template with the CoOOH nanoflakes. As expected, EXPAR using an

unmodified template alone produced long DNAs too large to enter the gel in all negative reactions that contained either no target miRNA or missing one of the enzymes (ESM Fig. S4a). These long products would generate high fluorescence with the reaction detected by SYBR Gold™ in the real-time PCR instrument.

The nonspecific strand extension could be from intra and intermolecular hybridization of templates, producing a short and random double-stranded region that primes polymerase activity. Thus, dissociating the single-stranded template and the polymerase by ssDNA-binding nanomaterials may be one effective way of suppressing background. Supplementing the reaction with CoOOH nanoflakes apparently decreased the production of the long DNA (ESM Fig. S4b). Another typical way to reduce background in isothermal amplifications is to block the 3’ OH end of the template with chemical modification. We found that the hexanediol modification effectively reduced background production, but product generation also decreased (ESM Fig. S4c). Interestingly, compared to the slight advantages brought by the CoOOH nanoflakes or by the hexanediol modification alone, we observed strong synergistic effects when combining these two chemical (hexanediol) and physical (nanoflakes) blocking approaches: the product band greatly intensified with negligible background detected in the negative reactions (Figure 3a). The exact reason behind the synergistic effect between the hexanediol modification and CoOOH nanoflakes in blocking non-specific target extension in our EXPAR design is not known. We hypothesize that the extensive hydrogen bonds between the hexanediol and the perhydroxyl groups on the nanoflake surface may create a stable and concentrated locale of templates on the nanoflakes and enhance amplification.

Inspired by the synergistic effects of the nanoflakes and hexanediol modification, we employed another physical blockage using single-stranded DNA-binding proteins (SSB) [67], which has been employed in PCR to help preserve the ssDNA structure and promote enzyme access. T4 gene 32 protein (T4 gp32)[68,69] is an economical alternative to the general SSB used in PCR, and thus selected in our assay. The reactions were monitored in a real-time PCR instrument. Signal-to-noise (S/N) ratios were derived from amplification curves and used as an index of comparison among different treatment conditions: with no additives, with T4 gp32 only, with nanoflakes only, or with both T4 gp32 and nanoflakes, all using the hexanediol-modified template and targeting *miR-122.* The EXPAR results clearly revealed that combining the hexanediol modification with physical blockage using either the nanoflakes or T4 gp32 could improve the S/N by about 10 or 100 folds, respectively; however, employment of both physical blockage approaches with hexanediol presented a striking performance boost that increased the S/N by approximately 400 folds (ESM Fig. S5).

### Comparison with other modifications.

To further explore this surprising phenomenon, we tested other chemical modifications on the template when used together with CoOOH nanoflakes and T4 gp32. Phosphorylation of the 3’ end is commonly employed in normal EXPAR and other strand-displacement dependent isothermal amplification methods; but some reports also suggest that such a modification could be ineffective[19,70]. Relocating the nucleophilic 3’ OH to the 5’

position in the inverted dT base[71] should block template self-extension as well, but has not been thoroughly investigated for potentially blocking non-specific 3' extension. We compared background and positive signal generation on templates that are either unmodified or modified with phosphorylation, hexanediol or inverted dT and observed that the other two modifications failed to deliver any synergistic effect as that obtained with the 3'-hexanediol modification (Figure 3 b).

Not only did the hexanediol modification combined with nanoflakes and T4 gp32 yield a much higher S/N ratio than other modifications, but this combination offered much better specificity when non-specific miRNA targets, like *miR-16, miR-21*, and three *miR-122* mutants, were investigated. The 21- or 23-mer *miR-122* mutants are the results of *miR-122* maturation in the liver. They differ from the wild type *miR-122* by a single nucleotide: the 21-mer and 23-mer mutants are with 3' G deletion and 3' adenylation, respectively[72,73]. The ratio of mutant levels may dictate the onset of a corresponding liver disease. We also included a custom miR-122 isoform containing a center point mutation to increase the stringency of our specificity test. Minimal signal was obtained from miR-16 and -21, and the 23-mer mutant of miR-122, which had an extra A on the 3' end to promote DNA breathing and compromise the double-stranded substrate needed for favorable polymerase binding. However, the 21-mer mutant with a missing G at the 3' end and the mutant with one nucleotide difference at the center position also generated positive signals, although lower than that of wild type *miR*-122, probably because their 3'-end region could still stably hybridize to the template to initiate polymerization.

Distinction of these mutants with high sequence similarity to the target strand should be solved by other template designs in future studies. In this work, we briefly attempted the strategy of using a hairpin template, which has been reported to be able to enhance target specificity compared to a linear ones[29,74]. We designed a hairpin template with a stem-loop that does not unfold in the presence of target. However, regardless of the 3' hexanediol's presence, the hairpin template failed to amplify appreciably (ESM Fig. S6).

### Comparison with other nanomaterials.

Other ssDNA-binding nanomaterials may adsorb the template and improve the performance of EXPAR as well. We therefore compared the EXPAR results obtained by CoOOH nanoflakes, gold nanospheres (AuNP) or graphene oxide (GO). Both AuNP and GO are popular substrates in many nanomaterial-facilitated isothermal applications. In lieu of nanoflakes, the citrate-capped gold nanospheres with an average diameter of 15 nm (nanoComposix) and GO sheets (diameter of 465 ± 155 nm and thickness 0.85 – 1.1 nm and zeta-potential of −46.6 ±1.4 mV; detailed characterization can be found in [41,42]) were tested as well for their performance in EXPAR. They were concentrated by centrifugation at 10,000 RCF and reconstituted to an appropriate concentration for EXPAR. These nanomaterials then substituted the nanoflakes in EXPAR with 40 nM of 3'-hexanediol template. The reactions using AuNPs or GO were optimized to get their best performance. Still, we found that the CoOOH nanoflakes outperformed AuNPs and GO in EXPAR (Figure 3c). We hypothesize that this may be attributed to 1) the better water solubility of CoOOH compared to GO and 2) the larger specific surface area of the 2D CoOOH nanoflake than

that of the AuNPs. Both these properties allow the nanoflakes to offer more protection against nonspecific polymerase activity than the surfaces of the other two nanomaterials.

### Detection sensitivity and cross-reactivity with other miRNAs.

Because the allied combination of hexanediol, nanoflakes, and T4 gp32 leads to superior S/N enhancement and satisfactory specificity, these modifications collectively established our working EXPAR system. Thus, the final system of the template-blocking EXPAR contains *Bst* 2.0, hexanediol-modified template, CoOOH nanoflakes and T4 gp32. It was tested for detection of *miR*-122. The assay sensitivity was evaluated by monitoring the reactions over the target concentration range of 500 fM to 50 aM by the CFX Connect Real-Time PCR Detection System with the $C_q$'s (quantitation cycle) obtained using the CFX manager software. Excellent linearity and reproducibility were achieved over at least 5 orders of magnitude (Figure 4). Defining the detection limit as $\bar{x} - 3s$, where $\bar{x}$ and s are respectively the mean and standard deviation of the blank, the LoD computes to $C_q = 35.28$, which translates to 151 ymol or 7.58 aM using the regression formula. Compared to other isothermal methods for miRNA detection[75], this method's LoD is at least one order of magnitude lower and well below the levels found in circulation[43,44]. This is a significant improvement over conventional EXPAR and LAMP, both of which are notorious for high levels of background amplification[17]. Along the same line, RCA, SDA, HCR, or DSNSA (duplex-specific nuclease signal amplification) are other notable isothermal systems that generally have detection limits within only 10 – 100 fM[75].

The specificity of the template-blocking EXPAR over strands with single mutations at the same concentration as the wild type target has been shown in Figure 3b. In the present performance evaluation, we mainly focused on the cross-reactivity against other non-target miRNAs. The test was further challenged by setting the concentration of non-targets ten times greater than *miR*-122, which was at 50 aM. As shown in Figure 4c (amplification curves shown in ESM Fig. S7a), only *miR*-122 produced a significant response above noise, whereas non-target strands were below. Cross-reactivity was also subjected to a more natural milieu using a mixture of *miR*-122 and non-targets at equimolar concentrations. Under these criteria, the template-blocking EXPAR was still able to selectively amplify *miR*-122 and curb false positives from *miR*-16, *miR*-21 and *miR*-191 (Figure 4d; amplification curves shown in ESM Fig. S7b). Together, these results established that this EXPAR system holds satisfactory performance towards detecting at low abundance and differentiating the target miRNA from other non-target ones.

### EXPAR detection of other miRNA targets.

To confirm that our CoOOH nanoflake-assisted EXPAR can be applied to detect other miRNA targets, we designed the appropriate templates for *miR*-16 and *miR*-21. Detection specificity was evaluated by reacting *miR*-16, *miR*-21, *miR*-122, and *miR*-191 with either the *miR*-16 template or *miR*-21 template and comparing the resulting EXPAR signals. To further challenge the assay, the target of interest was set at 50 aM while the non-target strands were at 500 aM.

Specific *miR*-16 EXPAR was easily met under these conditions and its specificity profile presents a highly selective reaction (Figure 5a; amplification curves in ESM Fig. S8a). *miR*-21 EXPAR was found to be specific also, but emitted a weaker positive signal than *miR*-16 EXPAR (Figure 5b; amplification curves in ESM Fig. S8b). The stronger amplification of *miR*-16 can be ascribed to the strand's 3' end being more GC-rich than *miR-2Vs*, effectively reducing DNA breathing and allowing better polymerase binding. However, it is interesting to note that *miR*-16 and -21 EXPAR also required 8× less *Bst* 2.0 than that of *mil*-122 EXPAR in order to evade high background generation and implement proper detection. This observation is in accordance with our own reverse transcription RT-qPCR protocol, where *miR*-16 and -21 are quickly detectable with less polymerase but *miR*-122 demands 2× as much.

### Detection of target miRNA in serum.

Serum detection of miRNA is the culmination of every optimization, refinement and critical attempt at background reduction. However, direct application of the developed EXPAR assay to detect miRNA in serum could be inhibited by the highly complex serum matrix[11,12]. Several protocol adjustments were introduced in order to transition from a clean buffer system to the physiological environment of serum. First, the serum was clarified of large particle debris (e.g., precipitated lipids and lipoproteins) so that they would not saturate the surface of nanoflakes that were subsequently added. Besides playing the ancillary role of enhancing signal-to-noise ratio, the nanoflakes also can enrich RNAs in serum by adsorbing and isolating the total nucleic acids from the sample. The EXPAR detection solution would then be added directly to the nanoflakes to amplify the target strands among the adsorbed total RNAs (Figure 1a). More nanoflakes were used compared to in-water detection to avoid incomplete target capture. This situation underlies from the fact that serum embodies a larger ensemble of endogenous nucleic acid species that will compete for nanoflake adsorption[11]. As a side effect of extra nano flakes, the reaction requires more amplification cycles to rise above background, as indicated by the higher $C_q$ scale (Figure 4b vs. Figure 6a), due to the greater adsorption dynamic between nanoflakes and newly synthesized EXPAR products.

To simulate circulating miRNA and validate the method's capability to handle such targets, *miR*-122-spiked serum samples were prepared and analyzed. Evidenced by the amplification curves, serum detection becomes increasingly difficult as concentration approaches background (Figure 6a), although linearity can still be constituted over at least 6 orders of magnitude between 500 pM – 5 fM (Figure 6b). This range encompasses that of circulating miRNA concentrations [43,44] and highlights the extent of our nanoflake-assisted EXPAR method to undertake serum detection.

## Conclusions

In the present day and age of unpredictable cancer incidences, there is very much a high demand for rapid and sensitive assays for biofluid biomarkers, which can be used to guide early disease detection and appropriate treatment. The analytical development of this work focuses on enabling detection of circulating miRNA through EXPAR. Consequently, several

cogent strategies were executed to mitigate background generation. Among them, the CoOOH nanoflakes are focal in our design and responsible for enriching target miRNAs and shielding free template from premature polymerase interactions. Equally important are the background-reducing effects of the hexanediol modification and T4 gp32, which respectively block DNA polymerase elongation and reinforce the linear structure of the template. We envision that our template-blocked EXPAR system fits the need of minimally invasive point-of-care diagnosis. By virtue of the advantages brought about in this work, it is with utmost optimism that the proposed EXPAR assay will motivate further biomarker discovery and advance mankind's campaign against cancer.

Many enzymatic isothermal amplification strategies, including EXPAR, are lacking specificity over strands with very high sequence similarity, which was also observed in our work. However, their fast reaction speed and high sensitivity are still valuable in rapidly screening the presence of target miRNAs or those with similar sequences in biological samples. Detection of the expression profiles of strands with single or multiple mutations could then be followed if needed. We also believe that the hydrogen bonding interactions between the hexanediol template and nanoflake substrate in this EXPAR system enforce more stringent template-target hybridization conditions and thereby ameliorate common specificity issues, while still maintaining the advantage of high enzyme processivity. Such a phenomenon is worthy of future study and may bring in benefits to other isothermal amplification strategies as well.

## Supplementary Material

Refer to Web version on PubMed Central for supplementary material.

## Acknowledgements

This work was supported by the National Institutes of Health grants R01-CA188991 and University of California Cancer Research Coordinating Committee, Grant ID #CRR-19585695, to W.Z. GO used in the research presented in this publication were developed, characterized, and provided by the Nanotechnology Health Implications Research Consortium established by the National Institute of Environmental Health Sciences (NIEHS) at Harvard T. H. Chan School of Public Health under the support of NIH grant No. U24ES026946.

## Biographies

**Michael Trinh** is a 5$^{th}$ year bioanalytical chemistry Ph.D. student at University of California, Riverside and earned his B.S. in chemistry at University of California, Berkeley. Currently, he is involved in developing isothermal detection platforms to profile circulating RNAs in serum.

**Jocelyn Carballo** was an undergraduate researcher in the Zhong lab and received her bachelor's degree in Chemistry at University of California, Riverside in June 2019. She participated in research projects about nanomaterial-based extraction and amplification of circulating miRNAs. She is currently working as a Heparin Chemist at Aaren Scientific, Inc.

**Gary Brent Adkins** is a 5$^{th}$ year graduate student at University of California, Riverside. He got his undergraduate degree from Austin Peay State University in Clarksville, TN. Throughout his tenure at UC Riverside, he has been developing methods using asymmetrical flow field flow fractionation and nanoparticle tracking analysis for the characterization of engineered and biological nanoparticles.

**Kaizhu Guo** is a Ph.D. student at University of California, Riverside. Her research is mainly focused on developing novel signaling strategies using DNA nanostructures to detect single vesicle biomarkers for disease diagnosis.

**Wenwan Zhong** is a Professor of Chemistry at University of California, Riverside. She completed her Ph.D. in Analytical Chemistry at Iowa State University and postdoctoral studies at Los Alamos National Laboratory before joining UCR, where she now leads and mentors her research team in three current focuses: 1) Rapid processing and detection of cell-free biomarkers from biospecimens for clinical applications; 2) Discovery of novel probes for epigenetic factors like histone post-translational modification and DNA methylation to study and/or control their biological functions in vitro and in vivo; and 3)

Study of the nano-bio interface to guide sustainable design and applications of nanomaterials.

## References


1. Ilie M, Hofman P Pros: Can tissue biopsy be replaced by liquid biopsy? Transl Lung Cancer Res. 2016, 5:420–423. [PubMed: 27655109]
2. Bartel DP MicroRNAs: target recognition and regulatory functions. Cell. 2009, 136:215–233. [PubMed: 19167326]
3. Guo H, Ingolia NT, Weissman JS, Bartel DP Mammalian microRNAs predominantly act to decrease target mRNA levels. Nature. 2010, 466:835–840. [PubMed: 20703300]
4. Lu J, Getz G, Miska EA, Alvarez-Saavedra E, Lamb J, Peck D, Sweet-Cordero A, Ebert BL, Mak RH, Ferrando AA, Downing JR, Jacks T, Horvitz HR, Golub TR MicroRNA expression profiles classify human cancers. Nature. 2005, 435:834–838. [PubMed: 15944708]
5. Palanichamy JK, Rao DS miRNA dysregulation in cancer: towards a mechanistic understanding. Front Genet. 2014, 5:54. [PubMed: 24672539]
6. Volinia S, Calin GA, Liu CG, Ambs S, Cimmino A, Petrocca F, Visone R, Iorio M, Roldo C, Ferracin M, Prueitt RL, Yanaihara N, Lanza G, Scarpa A, Vecchione A, Negrini M, Harris CC, Croce CM A microRNA expression signature of human solid tumors defines cancer gene targets. Proc Natl Acad Sci U S A. 2006, 103:2257–2261. [PubMed: 16461460]
7. Croce CM Causes and consequences of microRNA dysregulation in cancer. Nat Rev Genet. 2009, 10:704–714. [PubMed: 19763153]
8. Cheng L, Sharples RA, Scicluna BJ, Hill AF Exosomes provide a protective and enriched source of miRNA for biomarker profiling compared to intracellular and cell-free blood. J Extracell Vesicles. 2014, 3.
9. Ge Q, Zhou Y, Lu J, Bai Y, Xie X, Lu Z miRNA in plasma exosome is stable under different storage conditions. Molecules. 2014, 19:1568–1575. [PubMed: 24473213]
10. Turchinovich A, Weiz L, Langheinz A, Burwinkel B Characterization of extracellular circulating microRNA. Nucleic Acids Res. 2011, 39:7223–7233. [PubMed: 21609964]
11. Fleischhacker M, Schmidt B Circulating nucleic acids (CNAs) and cancer--a survey. Biochim Biophys Acta. 2007, 1775:181–232. [PubMed: 17137717]
12. Pieper R, Gatlin CL, Makusky AJ, Russo PS, Schatz CR, Miller SS, Su Q, McGrath AM, Estock MA, Parmar PP, Zhao M, Huang ST, Zhou J, Wang F, Esquer-Blasco R, Anderson NL, Taylor J, Steiner S The human serum proteome: display of nearly 3700 chromatographically separated protein spots on two-dimensional electrophoresis gels and identification of 325 distinct proteins. Proteomics. 2003, 3:1345–1364. [PubMed: 12872236]
13. Buermans HP, den Dunnen JT Next generation sequencing technology: Advances and applications. Biochim Biophys Acta. 2014, 1842:1932–1941. [PubMed: 24995601]
14. Draghici S, Khatri P, Eklund AC, Szallasi Z Reliability and reproducibility issues in DNA microarray measurements. Trends Genet. 2006, 22:101–109. [PubMed: 16380191]
15. Ouyang T, Liu Z, Han Z, Ge Q MicroRNA Detection Specificity: Recent Advances and Future Perspective. Anal Chem. 2019, 91:3179–3186. [PubMed: 30702270]
16. Valoczi A, Hornyik C, Varga N, Burgyan J, Kauppinen S, Havelda Z Sensitive and specific detection of microRNAs by northern blot analysis using LNA-modified oligonucleotide probes. Nucleic Acids Res. 2004, 32:e175. [PubMed: 15598818]
17. Zhao Y, Chen F, Li Q, Wang L, Fan C Isothermal Amplification of Nucleic Acids. Chem Rev. 2015, 115:12491–12545. [PubMed: 26551336]
18. Qian J, Ferguson TM, Shinde DN, Ramirez-Borrero AJ, Hintze A, Adami C, Niemz A Sequence dependence of isothermal DNA amplification via EXPAR. Nucleic Acids Res. 2012, 40:e87. [PubMed: 22416064]
19. Tan E, Erwin B, Dames S, Ferguson T, Buechel M, Irvine B, Voelkerding K, Niemz A Specific versus nonspecific isothermal DNA amplification through thermophilic polymerase and nicking enzyme activities. Biochemistry. 2008, 47:9987–9999. [PubMed: 18729381]

20. Wang J, Zou B, Rui J, Song Q, Kajiyama T, Kambara H, Zhou G Exponential amplification of DNA with very low background using graphene oxide and single-stranded binding protein to suppress non-specific amplification. Microchimica Acta. 2015, 182:1095–1101.
21. Zhang K, Kang DK, Ali MM, Liu L, Labanieh L, Lu M, Riazifar H, Nguyen TN, Zell JA, Digman MA, Gratton E, Li J, Zhao W Digital quantification of miRNA directly in plasma using integrated comprehensive droplet digital detection. Lab Chip. 2015, 15:4217–4226. [PubMed: 26387763]
22. Reid MS, Paliwoda RE, Zhang H, Le XC Reduction of Background Generated from Template-Template Hybridizations in the Exponential Amplification Reaction. Anal Chem. 2018, 90:11033–11039. [PubMed: 30099867]
23. Wang Q, Liu R, Yang X, Wang K, Zhu J, He L, Li Q Surface plasmon resonance biosensor for enzyme-free amplified microRNA detection based on gold nanoparticles and DNA supersandwich. Sensors and Actuators B: Chemical. 2016, 223:613–620.
24. Yin H, Zhou Y, Chen C, Zhu L, Ai S An electrochemical signal 'off-on' sensing platform for microRNA detection. Analyst. 2012, 137:1389–1395. [PubMed: 22311172]
25. Li RD, Yin BC, Ye BC Ultrasensitive, colorimetric detection of microRNAs based on isothermal exponential amplification reaction-assisted gold nanoparticle amplification. Biosens Bioelectron. 2016, 86:1011–1016. [PubMed: 27498329]
26. Liu B, Liu J Comprehensive Screen of Metal Oxide Nanoparticles for DNA Adsorption, Fluorescence Quenching, and Anion Discrimination. ACS Appl Mater Interfaces. 2015, 7:24833–24838. [PubMed: 26491955]
27. Liu B, Liu J Sensors and biosensors based on metal oxide nanomaterials. TrAC Trends in Analytical Chemistry. 2019, 121:115690.
28. Hong C, Baek A, Hah SS, Jung W, Kim DE Fluorometric Detection of MicroRNA Using Isothermal Gene Amplification and Graphene Oxide. Anal Chem. 2016, 88:2999–3003. [PubMed: 26902732]
29. Liu H, Li L, Wang Q, Duan L, Tang B Graphene fluorescence switch-based cooperative amplification: a sensitive and accurate method to detection microRNA. Anal Chem. 2014, 86:5487–5493. [PubMed: 24823448]
30. Li F, Liu X, Zhao B, Yan J, Li Q, Aldalbahi A, Shi J, Song S, Fan C, Wang L Graphene Nanoprobes for Real-Time Monitoring of Isothermal Nucleic Acid Amplification. ACS Appl Mater Interfaces. 2017, 9:15245–15253. [PubMed: 28414417]
31. Shuai HL, Huang KJ, Chen YX, Fang LX, Jia MP Au nanoparticles/hollow molybdenum disulfide microcubes based biosensor for microRNA-21 detection coupled with duplex-specific nuclease and enzyme signal amplification. Biosens Bioelectron. 2017, 89:989–997. [PubMed: 27825521]
32. Su S, Cao W, Liu W, Lu Z, Zhu D, Chao J, Weng L, Wang L, Fan C, Wang L Dual-mode electrochemical analysis of microRNA-21 using gold nanoparticle-decorated MoS2 nanosheet. Biosens Bioelectron. 2017, 94:552–559. [PubMed: 28363193]
33. Huang K-J, Shuai H-L, Chen Y-X Layered molybdenum selenide stacking flower-like nanostructure coupled with guanine-rich DNA sequence for ultrasensitive ochratoxin A aptasensor application. Sensors and Actuators B: Chemical. 2016, 225:391–397.
34. Huang KJ, Liu YJ, Wang HB, Wang YY, Liu YM Sub-femtomolar DNA detection based on layered molybdenum disulfide/multi-walled carbon nanotube composites, Au nanoparticle and enzyme multiple signal amplification. Biosens Bioelectron. 2014, 55:195–202. [PubMed: 24384259]
35. Huang KJ, Shuai HL, Zhang JZ Ultrasensitive sensing platform for platelet-derived growth factor BB detection based on layered molybdenum selenide-graphene composites and Exonuclease III assisted signal amplification. Biosens Bioelectron. 2016, 77:69–75. [PubMed: 26386905]
36. Wang YH, Huang KJ, Wu X Recent advances in transition-metal dichalcogenides based electrochemical biosensors: A review. Biosens Bioelectron. 2017, 97:305–316. [PubMed: 28618367]
37. Chang Y, Zhang Z, Liu H, Wang N, Tang J Cobalt oxyhydroxide nanoflake based fluorescence sensing platform for label-free detection of DNA. Analyst. 2016, 141:4719–4724. [PubMed: 27251111]

38. Cen Y, Yang Y, Yu RQ, Chen TT, Chu X A cobalt oxyhydroxide nanoflake-based nanoprobe for the sensitive fluorescence detection of T4 polynucleotide kinase activity and inhibition. Nanoscale. 2016, 8:8202–8209. [PubMed: 27030367]
39. Wang YM, Liu JW, Jiang JH, Zhong W Cobalt oxyhydroxide nanoflakes with intrinsic peroxidase catalytic activity and their application to serum glucose detection. Anal Bioanal Chem. 2017, 409:4225–4232. [PubMed: 28493021]
40. Van Ness J, Van Ness LK, Galas DJ Isothermal reactions for the amplification of oligonucleotides. Proc Natl Acad Sci U S A. 2003, 100:4504–4509. [PubMed: 12679520]
41. Parviz D, Strano M Endotoxin-Free Preparation of Graphene Oxide and Graphene-Based Materials for Biological Applications. Curr Protoc Chem Biol. 2018, 10:e51. [PubMed: 30285316]
42. Bitounis D, Parviz D, Cao X, Amadei CA, Vecitis CD, Sunderland EM, Thrall BD, Fang M, Strano MS, Demokritou P Synthesis and physicochemical transformations of size-sorted graphene oxide during simulated digestion and its toxicological assessment against an in vitro model of the human intestinal epithelium. Submitted. 2020.
43. Mitchell PS, Parkin RK, Kroh EM, Fritz BR, Wyman SK, Pogosova-Agadjanyan EL, Peterson A, Noteboom J, O'Briant KC, Allen A, Lin DW, Urban N, Drescher CW, Knudsen BS, Stirewalt DL, Gentleman R, Vessella RL, Nelson PS, Martin DB, Tewari M Circulating microRNAs as stable blood-based markers for cancer detection. Proc Natl Acad Sci U S A. 2008, 105:10513–10518. [PubMed: 18663219]
44. Max KEA, Bertram K, Akat KM, Bogardus KA, Li J, Morozov P, Ben-Dov IZ, Li X, Weiss ZR, Azizian A, Sopeyin A, Diacovo TG, Adamidi C, Williams Z, Tuschl T Human plasma and serum extracellular small RNA reference profiles and their clinical utility. Proc Natl Acad Sci U S A. 2018, 115:E5334–E5343. [PubMed: 29777089]
45. Kutay H, Bai S, Datta J, Motiwala T, Pogribny I, Frankel W, Jacob ST, Ghoshal K Downregulation of miR-122 in the rodent and human hepatocellular carcinomas. J Cell Biochem. 2006, 99:671–678. [PubMed: 16924677]
46. Coulouarn C, Factor VM, Andersen JB, Durkin ME, Thorgeirsson SS Loss of miR-122 expression in liver cancer correlates with suppression of the hepatic phenotype and gain of metastatic properties. Oncogene. 2009, 28:3526–3536. [PubMed: 19617899]
47. Tsai WC, Hsu PW, Lai TC, Chau GY, Lin CW, Chen CM, Lin CD, Liao YL, Wang JL, Chau YP, Hsu MT, Hsiao M, Huang HD, Tsou AP MicroRNA-122, a tumor suppressor microRNA that regulates intrahepatic metastasis of hepatocellular carcinoma. Hepatology. 2009, 49:1571–1582. [PubMed: 19296470]
48. Fornari F, Gramantieri L, Giovannini C, Veronese A, Ferracin M, Sabbioni S, Calin GA, Grazi GL, Croce CM, Tavolari S, Chieco P, Negrini M, Bolondi L MiR-122/cyclin G1 interaction modulates p53 activity and affects doxorubicin sensitivity of human hepatocarcinoma cells. Cancer Res. 2009, 69:5761–5767. [PubMed: 19584283]
49. Jopling CL, Yi M, Lancaster AM, Lemon SM, Sarnow P Modulation of hepatitis C virus RNA abundance by a liver-specific MicroRNA. Science. 2005, 309:1577–1581. [PubMed: 16141076]
50. Song K, Han C, Dash S, Balart LA, Wu T MiR-122 in hepatitis B virus and hepatitis C virus dual infection. World J Hepatol. 2015, 7:498–506. [PubMed: 25848473]
51. Fong MY, Zhou W, Liu L, Alontaga AY, Chandra M, Ashby J, Chow A, O'Connor ST, Li S, Chin AR, Somlo G, Palomares M, Li Z, Tremblay JR, Tsuyada A, Sun G, Reid MA, Wu X, Swiderski P, Ren X, Shi Y, Kong M, Zhong W, Chen Y, Wang SE Breast-cancer-secreted miR-122 reprograms glucose metabolism in premetastatic niche to promote metastasis. Nat Cell Biol. 2015, 17:183–194. [PubMed: 25621950]
52. Wang B, Wang H, Yang Z MiR-122 inhibits cell proliferation and tumorigenesis of breast cancer by targeting IGF1R. PLoS One. 2012, 7:e47053. [PubMed: 23056576]
53. Rivas MA, Venturutti L, Huang YW, Schillaci R, Huang TH, Elizalde PV Downregulation of the tumor-suppressor miR-16 via progestin-mediated oncogenic signaling contributes to breast cancer development. Breast Cancer Res. 2012, 14:R77. [PubMed: 22583478]
54. Kumarswamy R, Volkmann I, Thum T Regulation and function of miRNA-21 in health and disease. RNA Biol. 2011, 8:706–713. [PubMed: 21712654]

55. Andriani F, Majorini MT, Mano M, Landoni E, Miceli R, Facchinetti F, Mensah M, Fontanella E, Dugo M, Giacca M, Pastorino U, Sozzi G, Delia D, Roz L, Lecis D MiR-16 regulates the pro-tumorigenic potential of lung fibroblasts through the inhibition of HGF production in an FGFR-1- and MEK1-dependent manner. J Hematol Oncol. 2018, 11:45. [PubMed: 29558956]
56. Chan JA, Krichevsky AM, Kosik KS MicroRNA-21 is an antiapoptotic factor in human glioblastoma cells. Cancer Res. 2005, 65:6029–6033. [PubMed: 16024602]
57. Ciafre SA, Galardi S, Mangiola A, Ferracin M, Liu CG, Sabatino G, Negrini M, Maira G, Croce CM, Farace MG Extensive modulation of a set of microRNAs in primary glioblastoma. Biochem Biophys Res Commun. 2005, 334:1351–1358. [PubMed: 16039986]
58. Markou A, Zavridou M, Lianidou ES miRNA-21 as a novel therapeutic target in lung cancer. Lung Cancer (Auckl). 2016, 7:19–27. [PubMed: 28210157]
59. Fang S, Lee HJ, Wark AW, Corn RM Attomole microarray detection of microRNAs by nanoparticle-amplified SPR imaging measurements of surface polyadenylation reactions. J Am Chem Soc. 2006, 128:14044–14046. [PubMed: 17061884]
60. Komori M, Komiya K, Shirakawa T, Morikawa TJ, Yoshimura T Measurement of microRNA with isothermal DNA amplification on fully automated immunoassay analyzers. Anal Bioanal Chem. 2019, 411:3789–3800. [PubMed: 31161320]
61. Miao X, Ning X, Li Z, Cheng Z Sensitive detection of miRNA by using hybridization chain reaction coupled with positively charged gold nanoparticles. Sci Rep. 2016, 6:32358. [PubMed: 27576601]
62. Wang D, Hu L, Zhou H, Abdel-Halim ES, Zhu J-J Molecular beacon structure mediated rolling circle amplification for ultrasensitive electrochemical detection of microRNA based on quantum dots tagging. Electrochemistry Communications. 2013, 33:80–83.
63. Yan L, Nakayama S, Yitbarek S, Greenfield I, Sintim HO Isothermal detection of RNA with restriction endonucleases. Chem Commun (Camb). 2011, 47:200–202. [PubMed: 20886171]
64. Zhang X, Liu C, Sun L, Duan X, Li Z Lab on a single microbead: an ultrasensitive detection strategy enabling microRNA analysis at the single-molecule level. Chem Sci. 2015, 6:6213–6218. [PubMed: 30090237]
65. Xu Y, Wang Y, Liu S, Yu J, Wang H, Guo Y, Huang J Ultrasensitive and rapid detection of miRNA with three-way junction structure-based trigger-assisted exponential enzymatic amplification. Biosens Bioelectron. 2016, 81:236–241. [PubMed: 26954789]
66. Yao B, Li J, Huang H, Sun C, Wang Z, Fan Y, Chang Q, Li S, Xi J Quantitative analysis of zeptomole microRNAs based on isothermal ramification amplification. RNA. 2009, 15:1787–1794. [PubMed: 19620236]
67. Meyer RR, Laine PS The single-stranded DNA-binding protein of Escherichia coli. Microbiol Rev. 1990, 54:342–380. [PubMed: 2087220]
68. Zhang Y, Tanner NA Author Correction: Isothermal Amplification of Long, Discrete DNA Fragments Facilitated by Single-Stranded Binding Protein. Sci Rep. 2018, 8:4156. [PubMed: 29500412]
69. Chen G, Dong J, Yuan Y, Li N, Huang X, Cui X, Tang Z A general solution for opening double-stranded DNA for isothermal amplification. Sci Rep. 2016, 6:34582. [PubMed: 27687498]
70. Reid MS, Le XC, Zhang H Exponential Isothermal Amplification of Nucleic Acids and Assays for Proteins, Cells, Small Molecules, and Enzyme Activities: An EXPAR Example. Angew Chem Int Ed Engl. 2018, 57:11856–11866. [PubMed: 29704305]
71. Hoser MJ, Mansukoski HK, Morrical SW, Eboigbodin KE Strand Invasion Based Amplification (SIBA(R)): a novel isothermal DNA amplification technology demonstrating high specificity and sensitivity for a single molecule of target analyte. PLoS One. 2014, 9:e112656. [PubMed: 25419812]
72. Valdmanis PN, Gu S, Chu K, Jin L, Zhang F, Munding EM, Zhang Y, Huang Y, Kutay H, Ghoshal K, Lisowski L, Kay MA RNA interference-induced hepatotoxicity results from loss of the first synthesized isoform of microRNA-122 in mice. Nat Med. 2016, 22:557–562. [PubMed: 27064447]

73. Valdmanis PN, Kim HK, Chu K, Zhang F, Xu J, Munding EM, Shen J, Kay MA miR-122 removal in the liver activates imprinted microRNAs and enables more effective microRNA-mediated gene repression. Nat Commun. 2018, 9:5321. [PubMed: 30552326]

74. Deng H, Zhou X, Liu Q, Li B, Liu H, Huang R, Xing D Paperfluidic Chip Device for Small RNA Extraction, Amplification, and Multiplexed Analysis. ACS Appl Mater Interfaces. 2017, 9:41151–41158. [PubMed: 29116747]

75. Wang Y-M, Trinh MP, Zheng Y, Guo K, Jimenez LA, Zhong W Analysis of circulating non-coding RNAs in a non-invasive and cost-effective manner. TrAC Trends in Analytical Chemistry. 2019, 117:242–262.

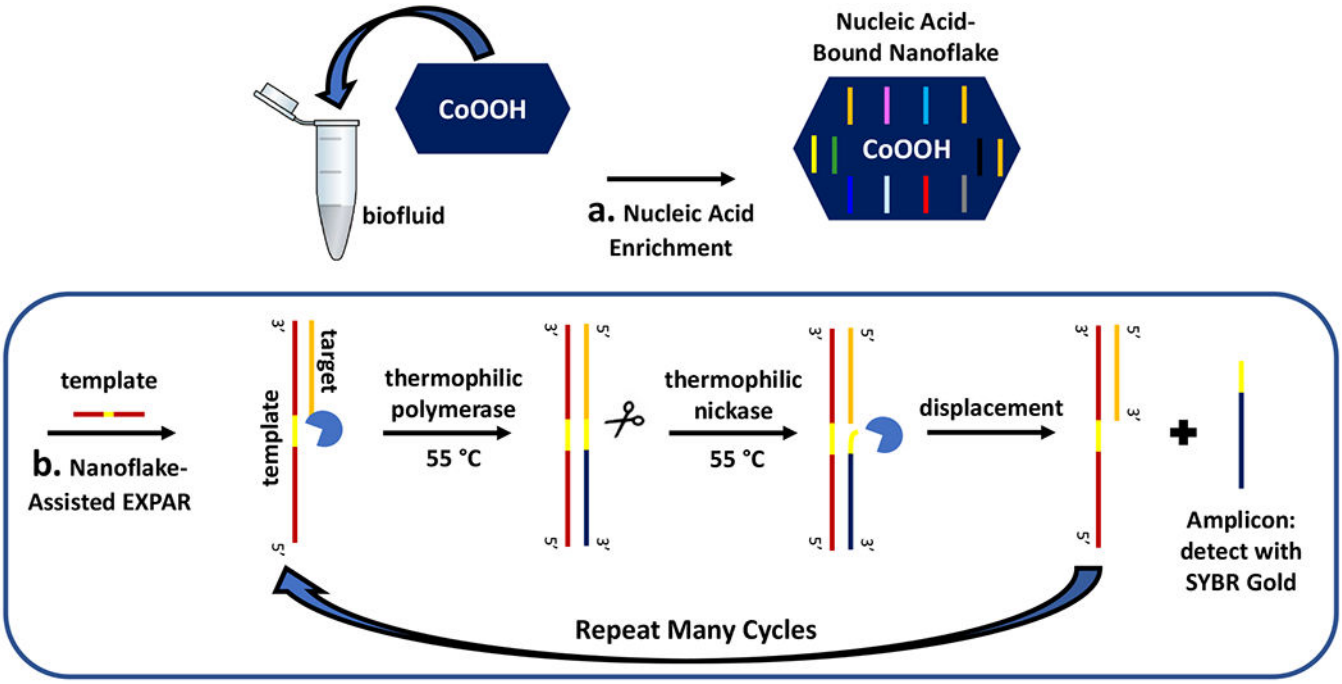


**Figure 1.**

Principle of circulating miRNA detection by template-blocking exponential amplification reaction (EXPAR). (a) Cobalt oxyhydroxide (CoOOH) nanoflakes are added to serum and recovered after incubation. (b) EXPAR is applied directly to target-bound nanoflakes and the resulting amplicon products are stained with SYBR Gold™ to generate amplification signal.

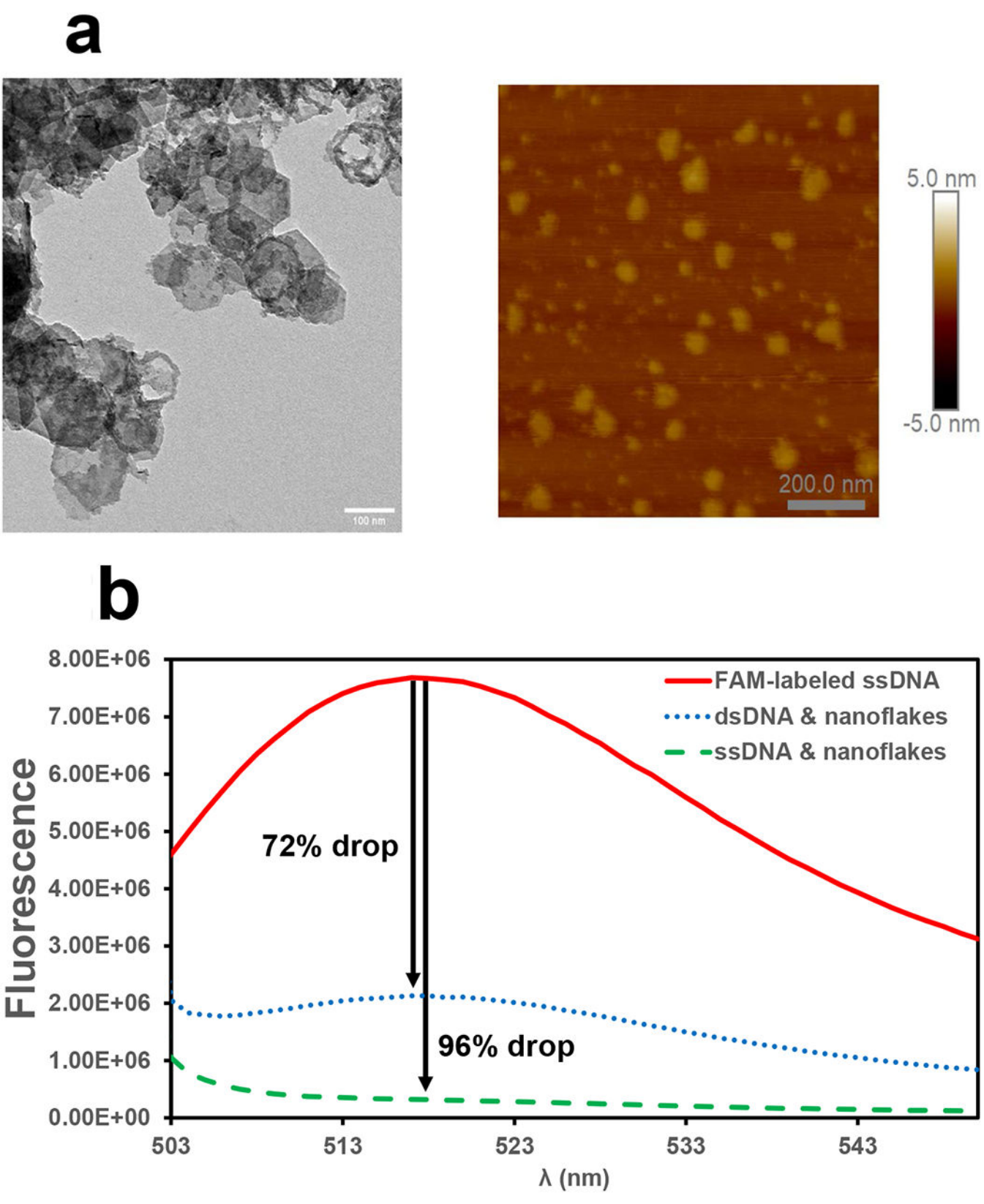


**Figure 2.**

Characterization of fabricated CoOOH nanoflakes. (a) TEM (left) and AFM (right) images of CoOOH nanoflakes. (b) Typical fluorescence spectra of FAM-labeled DNA capture probe with and without CoOOH nanoflakes. Maximum emission was measured at 520 nm for both single-stranded (ss) and double-stranded (ds) DNA.

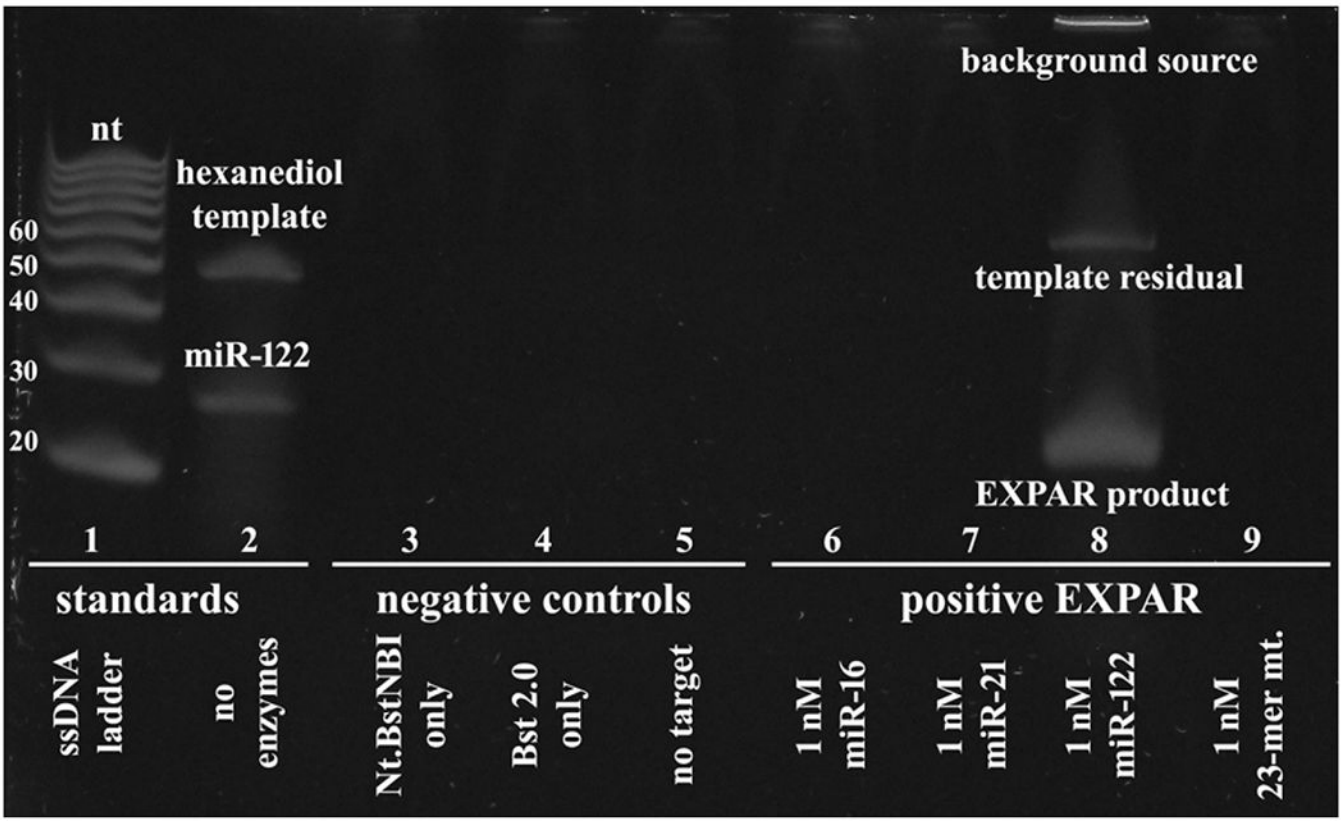

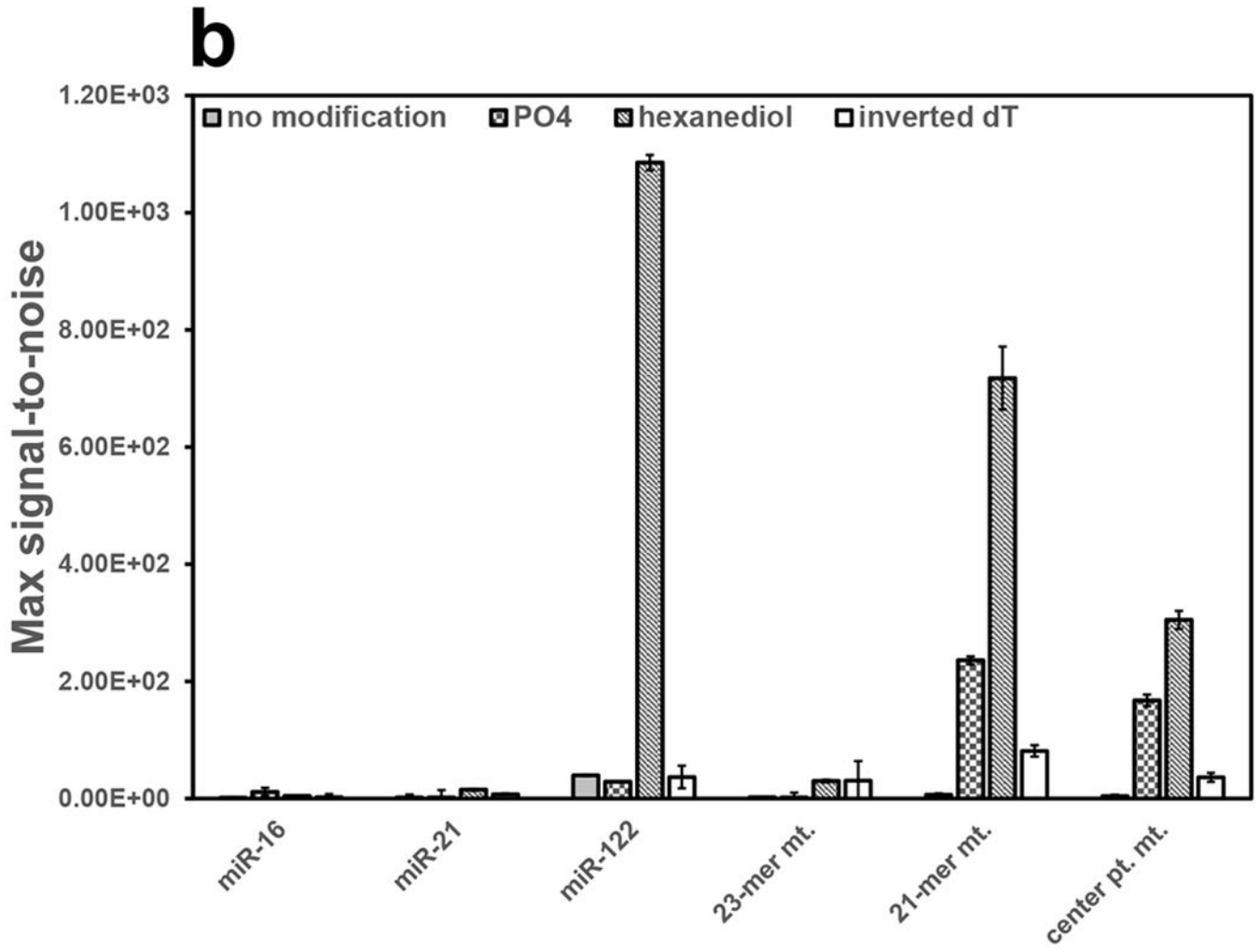

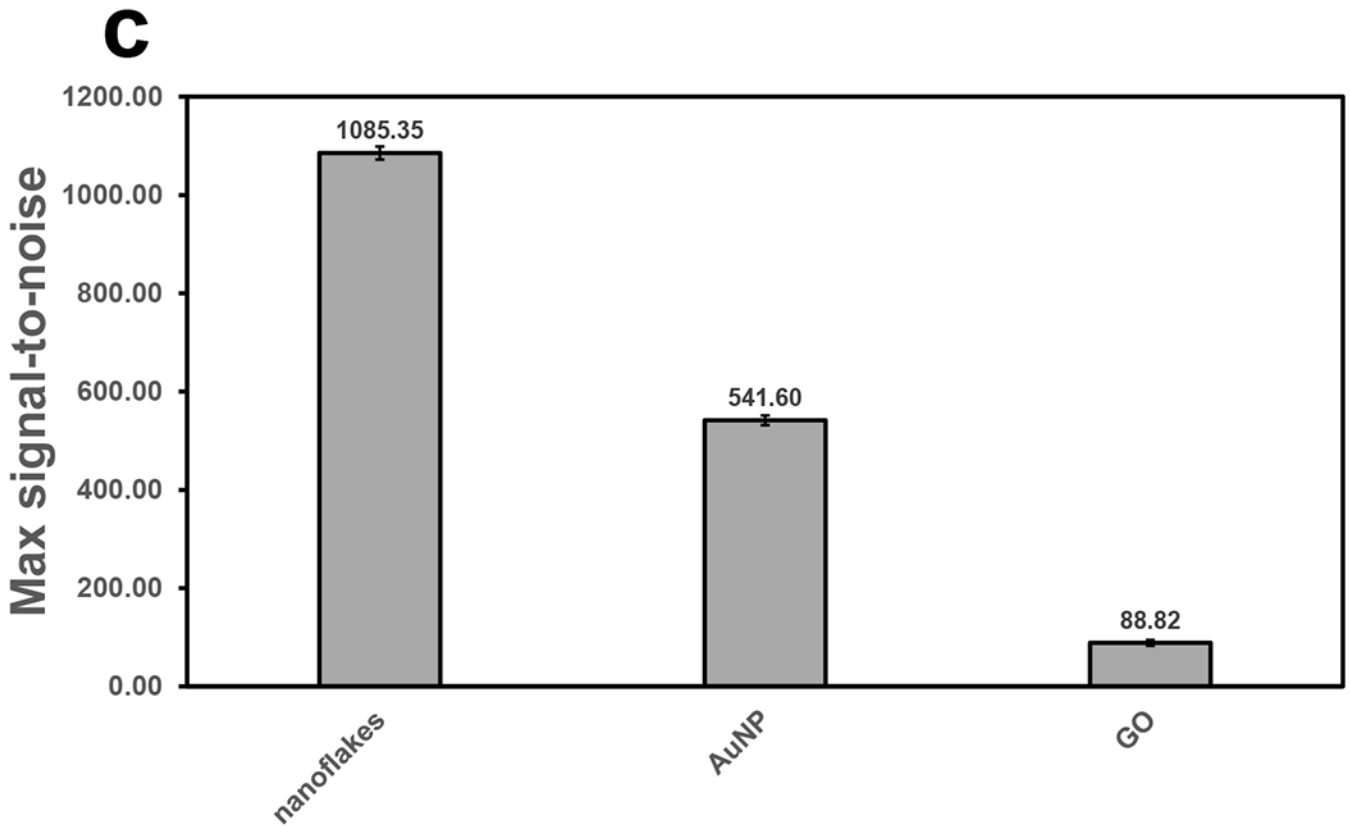


**Figure 3.**

Investigation of physical and chemical blockage of template. (a) Demonstration of the enhanced specificity attained for *miR*-122 EXPAR with the hexanediol-modified template and nanoflakes, as visualized by 20% denaturing PAGE, and with 1 nM of *miR*-122 in the negative controls. (b) Comparison of EXPAR results for detection of *miR*-122 with nanoflakes and templates carrying different 3' chemical modifications. Specificity was compared using the non-target strands of *miR*-16, *miR*-21, and several mutants of *miR*-122, with each miRNA strand at 500 aM. (c) Comparison of maximal S/N ratios produced by CoOOH nanoflakes and the two ssDNA-binding nanomaterials – GO and AuNPs – in *miR*-122 EXPAR using a 3' hexanediol-modified template, and 500 aM target. All error bars represent triplicate measurements.

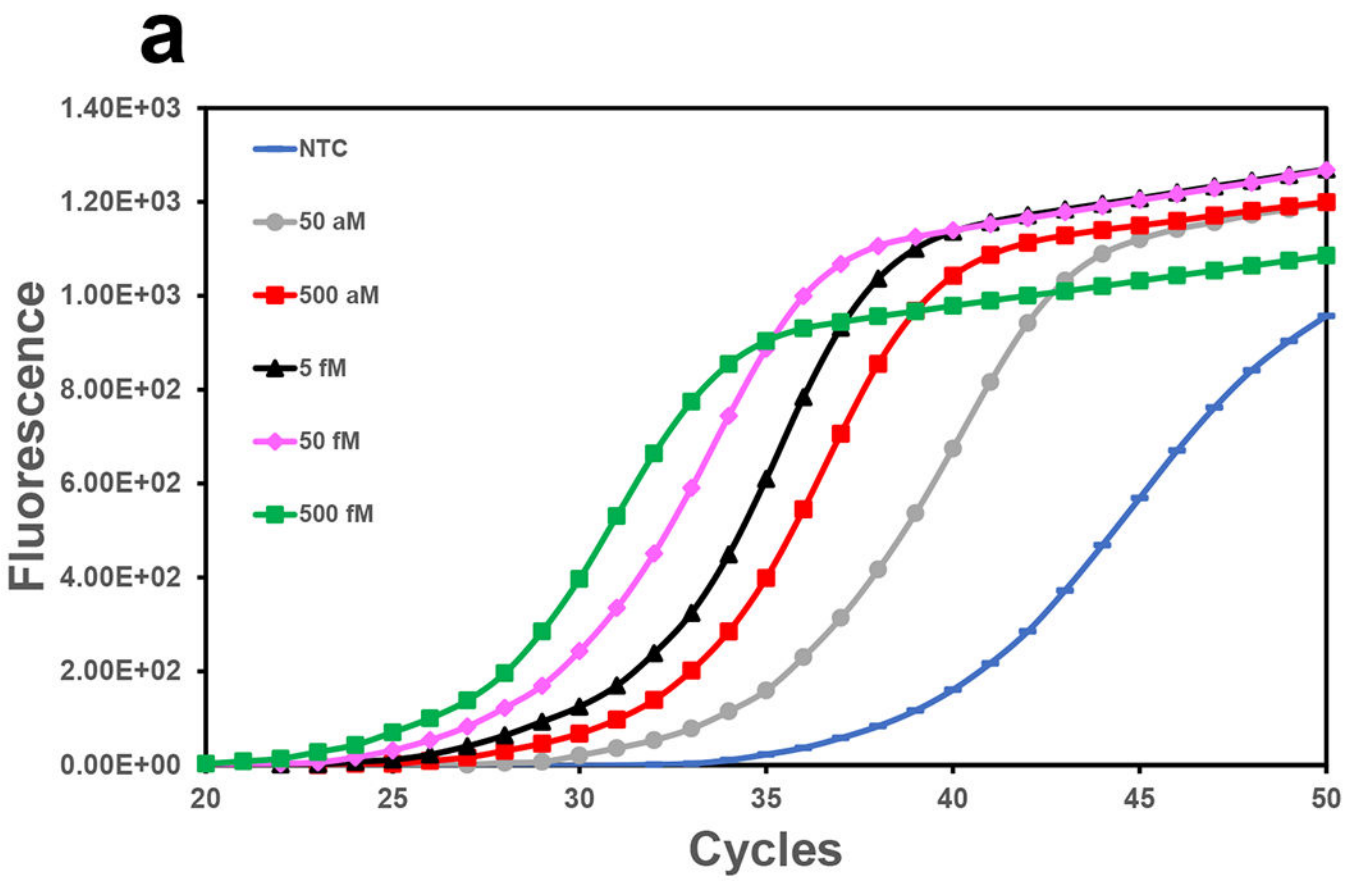

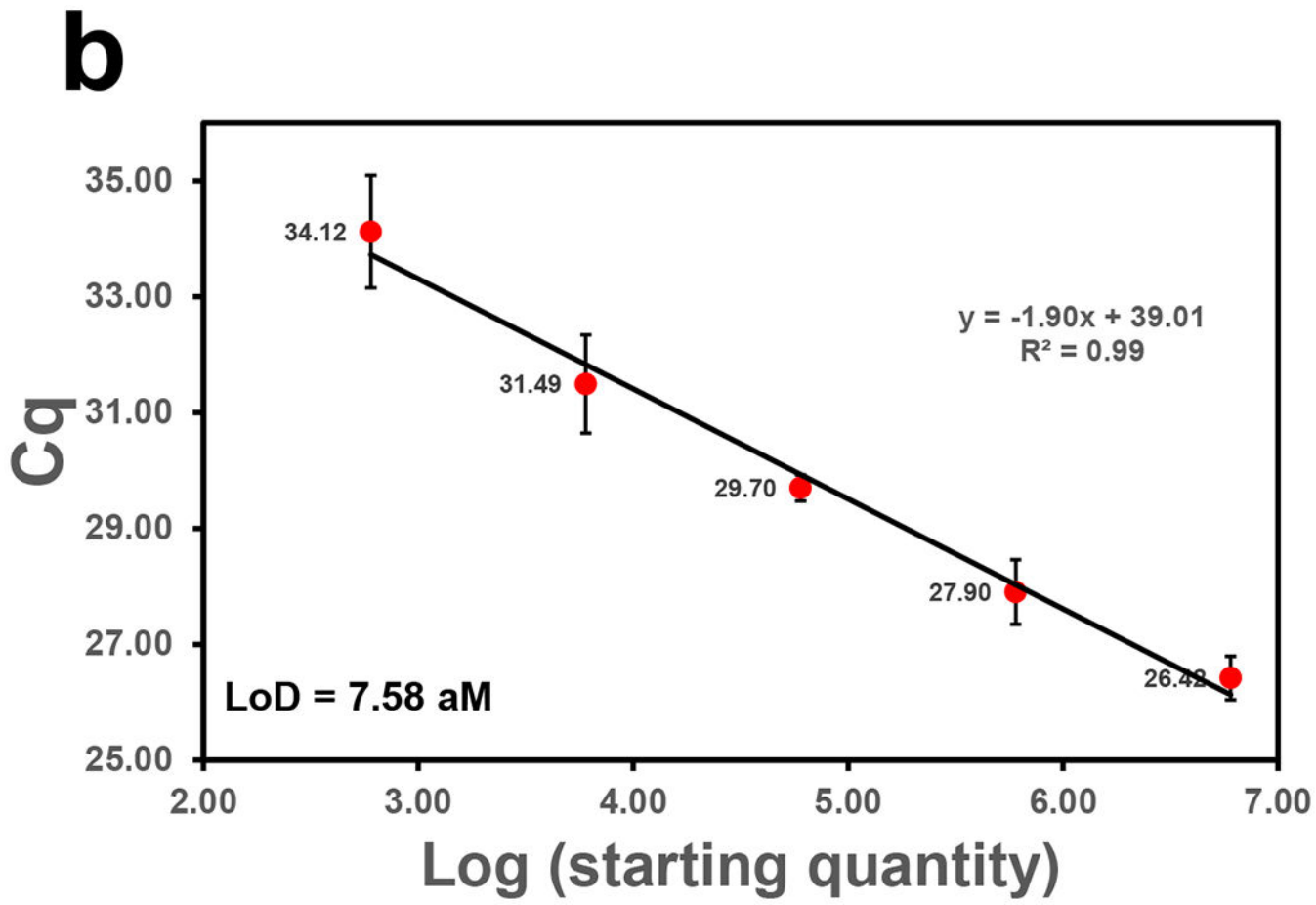

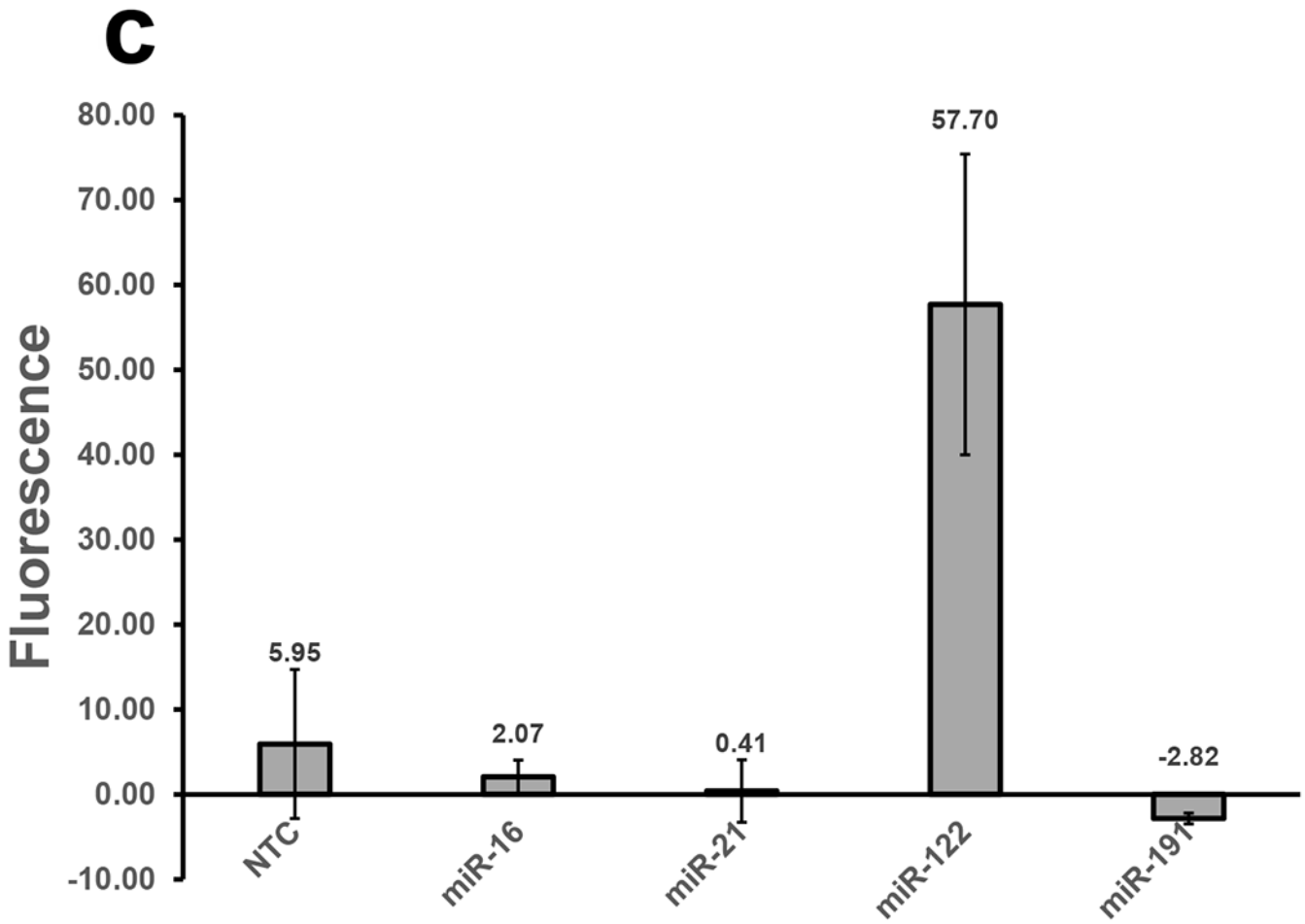

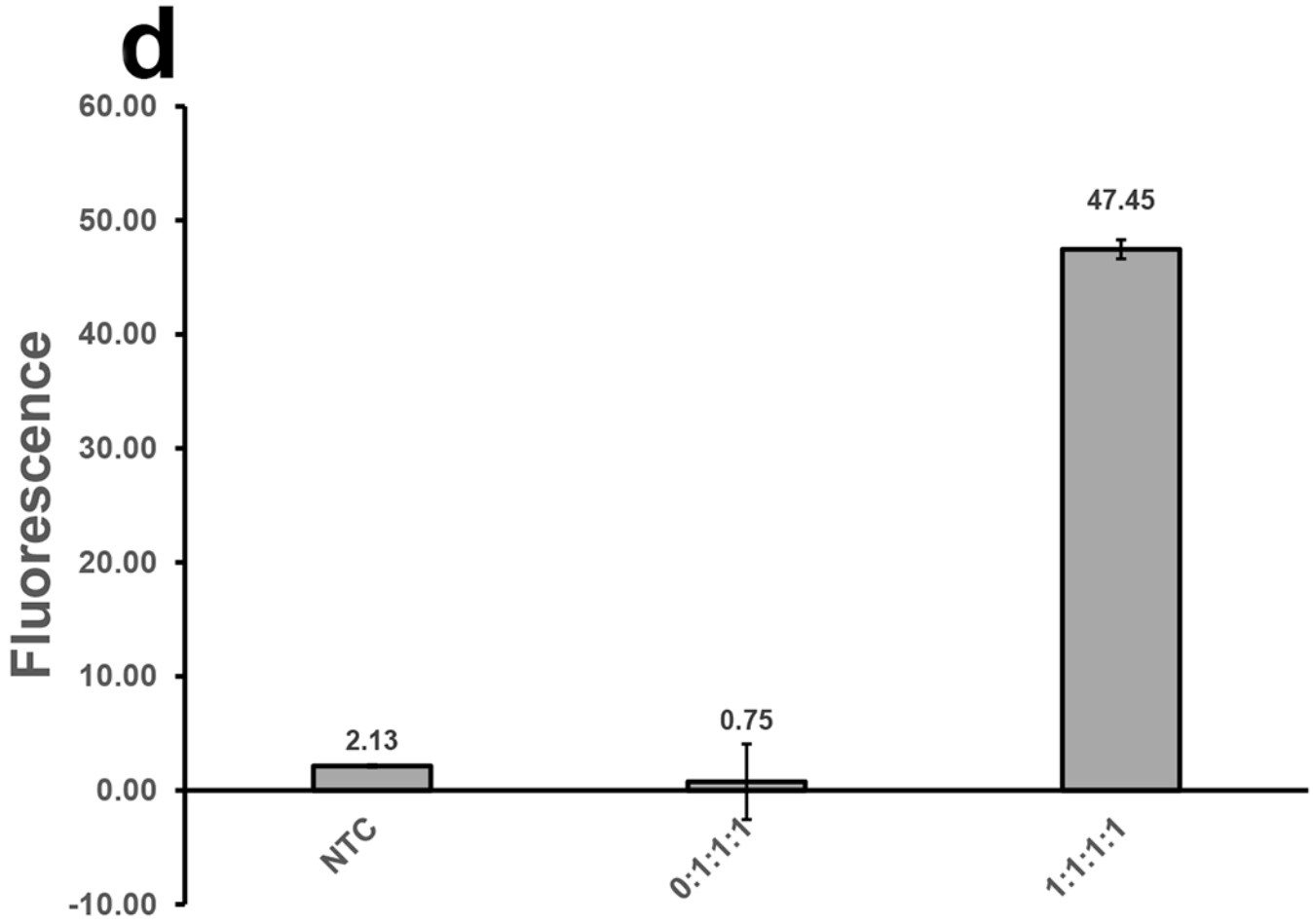


**Figure 4.**

(a) The linear regression and (b) standard amplification curves for the template-blocking EXPAR for detection of *miR*-122. Cross-reactivity was tested (c) against individual nonspecific strands and (d) in an equimolar mixture. In (c), *miR*-122 was set at 50 aM while non-target strands were at 500 aM. In (d), the ratio of 0:1:1:1 and 1:1:1:1 respectively represent 0 aM or 500 aM of miR-122 mixed with *miR*-16, *miR*-21 and *miR*-191, each at 500 aM. Amplification curves and error bars were recorded in triplicate. Target was denoted by (+), non-target strands by (X), and background by (−). NTC = no target control.

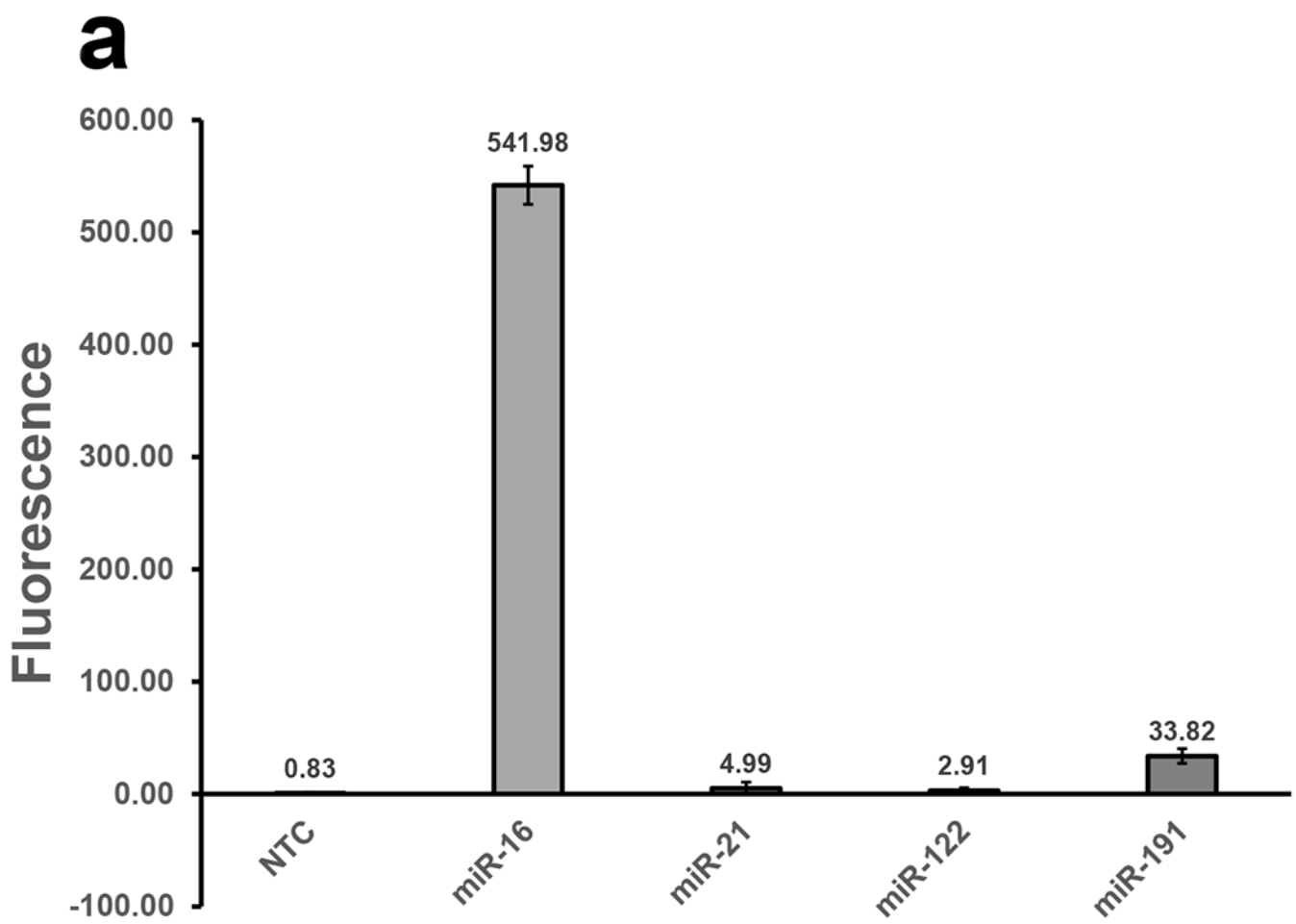

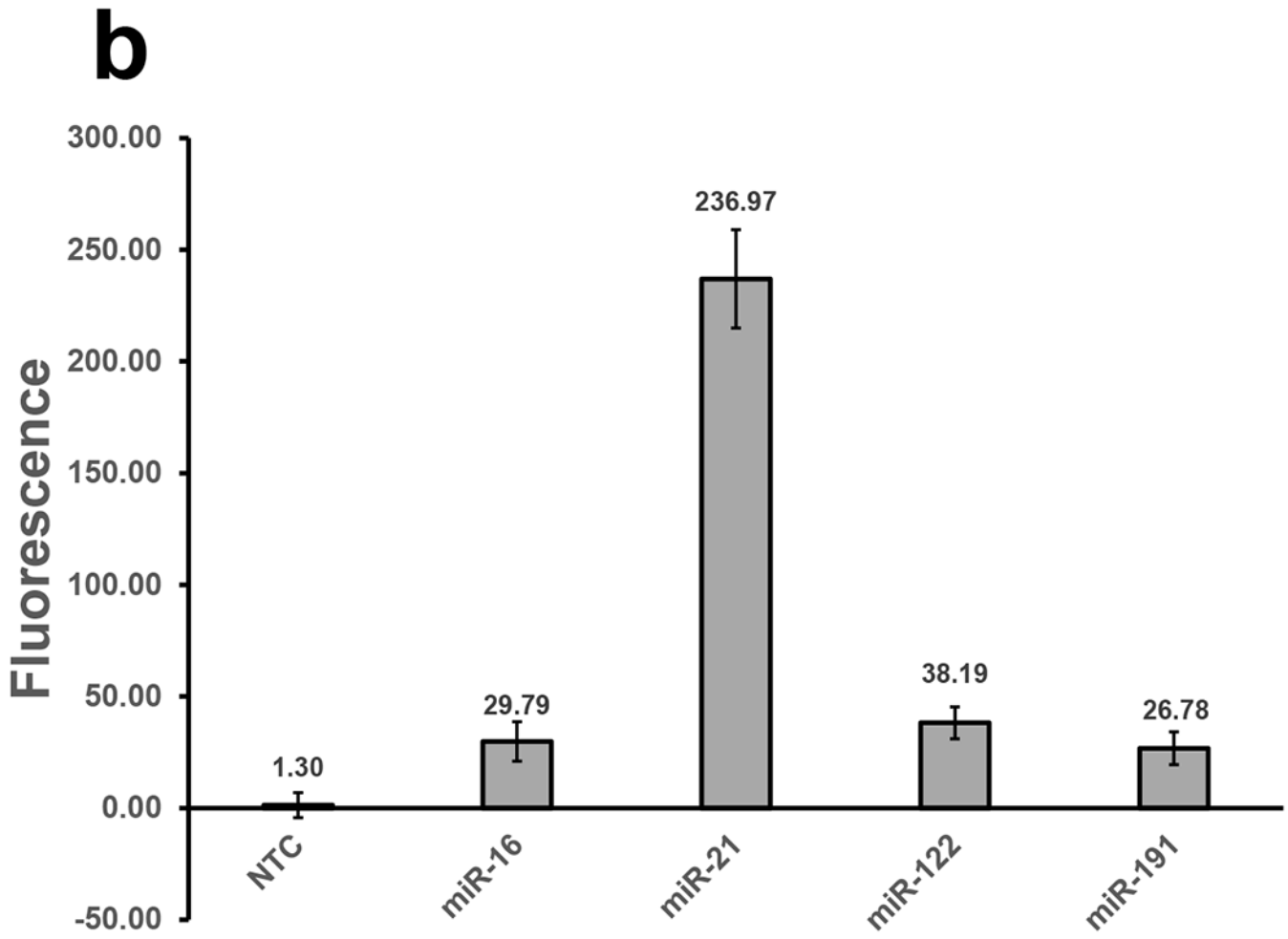


**Figure 5.**

Detection performance of (a) *miR*-16- and (b) *miR*-21-based template-blocking EXPAR. Target concentration was set at 50 aM while non-target strands were at 500 aM. Error bars represent triplicate measurements. NTC = no target control.

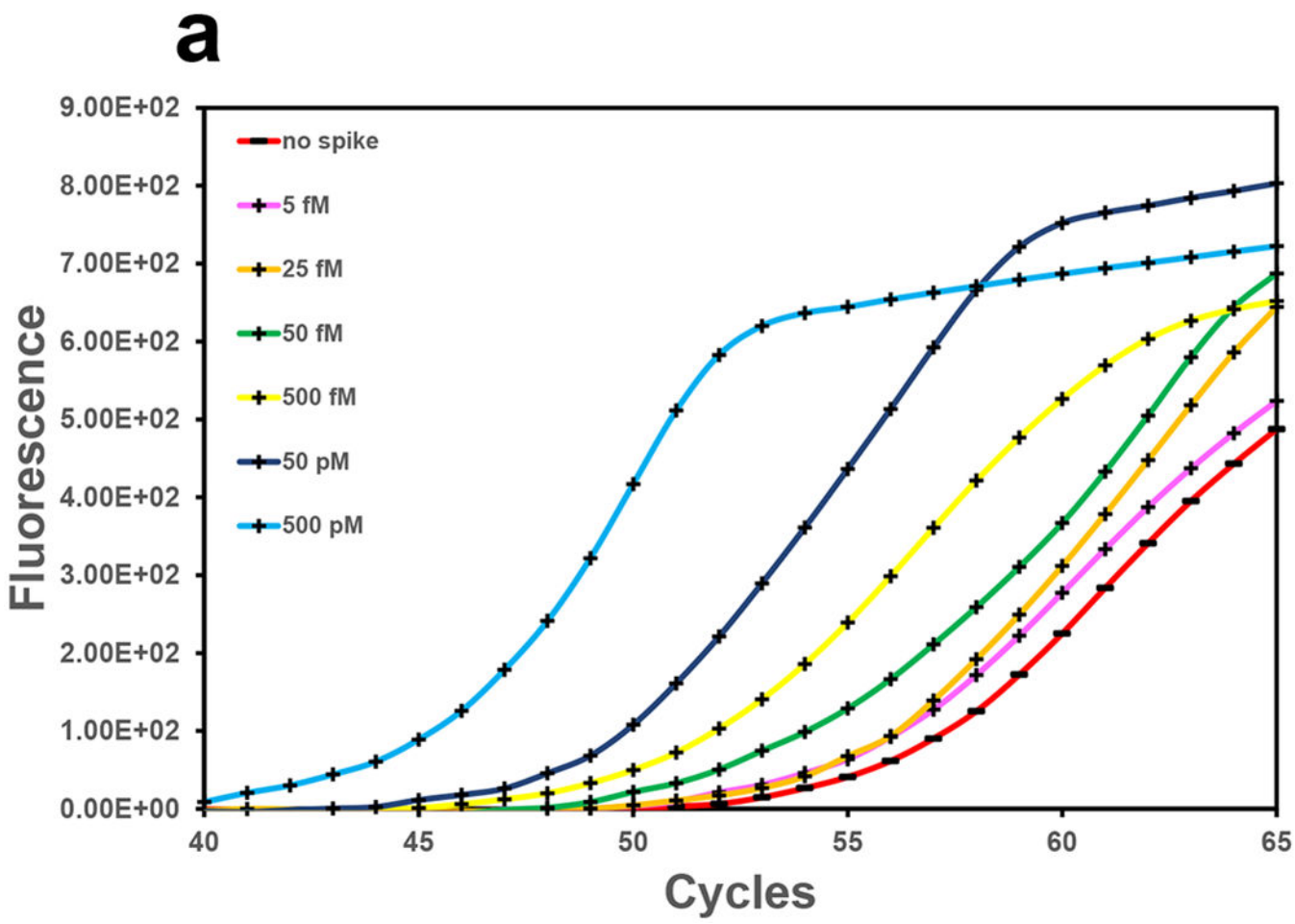

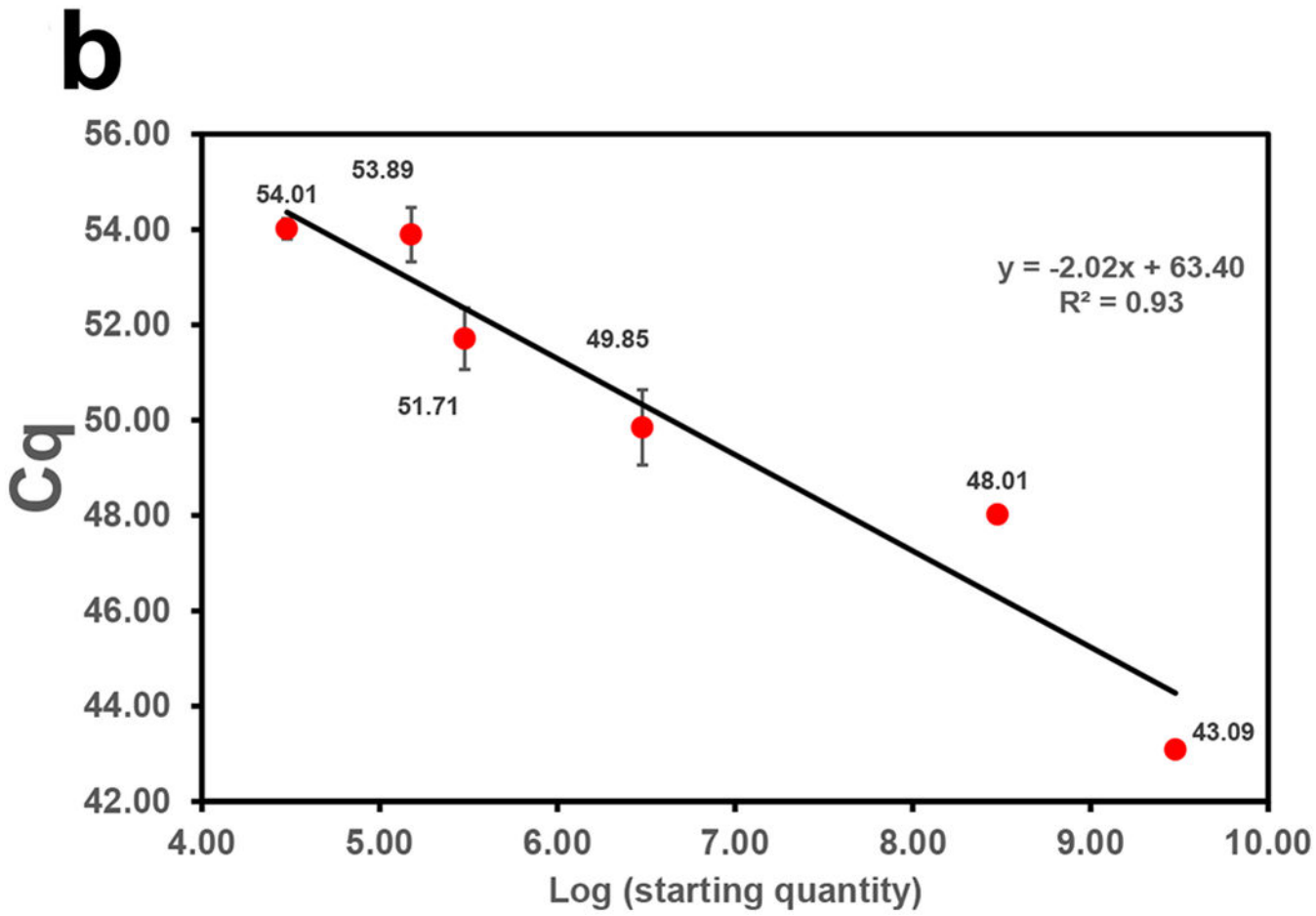


**Figure 6.**

(a) Amplification curves and (b) the calibration curve for detection of *miR*-122 spiked in healthy single donor human serum. In (a) (+) and (−) respectively referred to *miR*-122 and background. The indicated concentrations were the final concentrations after spiking into diluted serum. Error bars represent triplicate measurements.